Historical Biology
An International Journal of Paleobiology
Publication details, including instructions for authors and subscription information:
http://www.informaworld.com/smpp/title~content=t713717695

A nearly complete skeleton of an early juvenile diplodocid (Dinosauria: Sauropoda) from the Lower Morrison Formation (Late Jurassic) of north central Wyoming and its implications for early ontogeny and pneumaticity in sauropods

To cite this Article: Schwarz, Daniela, Ikejiri, Takehito, Breithaupt, Brent H., Sander, P. Martin and Klein, Nicole , 'A nearly complete skeleton of an early juvenile diplodocid (Dinosauria: Sauropoda) from the Lower Morrison Formation (Late Jurassic) of north central Wyoming and its implications for early ontogeny and pneumaticity in sauropods', Historical Biology, 19:3, 225 - 253
To link to this article: DOI: 10.1080/08912960601118651
URL: http://dx.doi.org/10.1080/08912960601118651

Historical Biology, 2007; 19(3): 225–253

A nearly complete skeleton of an early juvenile diplodocid (Dinosauria: Sauropoda) from the Lower Morrison Formation (Late Jurassic) of north central Wyoming and its implications for early ontogeny and pneumaticity in sauropods

DANIELA SCHWARZ[1], TAKEHITO IKEJIRI[2,†], BRENT H. BREITHAUPT[3,‡], P. MARTIN SANDER[4,¶], & NICOLE KLEIN[4,§]

[1]*Naturhistorisches Museum Basel, Augustinergasse 2, CH-4001 Basel, Switzerland,* [2]*Wyoming Dinosaur Center, 110 Carter Ranch Road, Thermopolis, WY 82443, USA,* [3]*Geological Museum, University of Wyoming, Laramie, WY 82071, USA, and* [4]*Institut für Paläontologie, Universität Bonn, Nussallee 8, D-53115 Bonn, Germany*

Abstract

A nearly complete skeleton of a juvenile sauropod from the Lower Morrison Formation (Late Jurassic, Kimmeridgian) of the Howe Ranch in Bighorn County, Wyoming is described. The specimen consists of articulated mid-cervical to mid-caudal vertebrae and most appendicular bones, but cranial and mandibular elements are missing. The shoulder height is approximately 67 cm, and the total body length is estimated to be less than 200 cm. Besides the body size, the following morphological features indicate that this specimen is an early juvenile; (1) unfused centra and neural arches in presacral, sacral and first to ninth caudal vertebrae, (2) unfused coracoid and scapula, (3) open coracoid foramen, and (4) relatively smooth articular surfaces on the limb, wrist, and ankle bones. A large scapula, short neck and tail and elongate forelimb bones relative to overall body size demonstrate relative growth. A thin-section of the mid-shaft of a femur shows a lack of annual growth lines, indicating an early juvenile individual possibly younger than a few years old. Pneumatic structures in the vertebral column of the specimen SMA 0009 show that pneumatisation of the postcranial skeleton had already started in this individual, giving new insights in the early ontogenetic development of vertebral pneumaticity in sauropods.

The specimen exhibits a number of diplodocid features (e.g., very elongate slender scapular blade with a gradually dorsoventrally expanded distal end, a total of nine dorsal vertebrae, presence of the posterior centroparapophyseal lamina in the posterior dorsal vertebrae). Although a few diplodocid taxa, *Diplodocus*, cf. *Apatosaurus*, and cf. *Barosaurus*, are known from several fossil sites near the Howe Ranch, identification of this specimen, even at a generic level, is difficult due to a large degree of ontogenetic variation.

Keywords: *Sauropod*, Diplodocidae, *Late Jurassic*, *taxonomy*, *early juvenile*, *ontogeny*

Institutional Abbreviations: *AMNH, American Museum of Natural History, New York; ANS, Academy of National Science Philadelphia, Pennsylvania; BHI, Black Hills Institution, Hill City, South Dakota; BYU, Brigham Young University Earth Science Museum, Provo, Utah; CM, Carnegie Museum of Natural History, Pittsburgh, Pennsylvania; DMNH, Denver Museum of Nature and Sciences, Denver, Colorado; MCW, Museum of Western Colorado, Fruita; MOR, Museum of the Rockies, Bozeman, Montana; NSMT-PV, National Science Museum, Tokyo; OMNH, Sam Noble Oklahoma Museum of Natural History, Norman; SMA, Sauriermuseum Aathal, Switzerland; USNM, National Museum of Natural History (formerly United States National Museum), Washington D.C.; WDC, Wyoming Dinosaur Center, Thermopolis; YPM, Yale Peabody Museum, New Haven, Connecticut*

Correspondence: D. Schwarz, Naturhistorisches Museum Basel, Augustinergasse 2, CH-4001 Basel, Switzerland.
E-mail: daniela.schwarz@bs.ch

[†]Current address: Museum of Paleontology and Department of Geological Sciences, The University of Michigan, 1109 Geddes Avenue, Ann Arbor, MI 48109-1079, USA. E-mail: ikejiri_t@hotmail.com

[‡]E-mail: uwgeoms@uwyo.edu

[¶]E-mail: m.sander@uni-bonn.de

[§]E-mail: nicole.f.klein@t-online.de

ISSN 0891-2963 print/ISSN 1029-2381 online © 2007 Taylor & Francis
DOI: 10.1080/08912960601118651

Anatomical Abbreviations: *acdl, anterior centrodiapophyseal lamina; acp, acromion process; acpl, anterior centroparapophyseal lamina; acr, acromion ridge; alp, anterolateral process of ulna; as, astragalus; asc, ascending process of astragalus; carp, carpal; Ca, caudal vertebra; cap, costal capitulum; captub cr, capitulotubercular crest of rib; cc, cnemial crest; Cep, posterior cervical vertebra; cefx, crus extensor fossa; cf, coracoid foramen; Che, chevron; cg, coracoidal glenoid; clav, clavicula; cor, coracoid; corp c, rib shaft; cprl, centroprezygapophyseal lamina; Cr, cervical rib; cr, crest; dep, depression; diap, diapophysis; Do, dorsal vertebra; Dor, dorsal rib; dpc, deltopectoral crest; dr, distal roller; ect, lateral epicondyle; fe, femur; fh, femoral head; fi, fibula; fib, fibular articular surface of astragalus; gt, greater trochanter; hu, humerus; idif, infradiapophyseal fossa; il, ilium; iprf, intraprezygapophyseal fossa; is, ischium; iscped, ischiac peduncle; isf, infrascapular fossa; lc, lateral condyle of femur; ldcr, lateral distal crest of humerus; lrug, lateral rugosity of fibula; lt, lesser trochanter; luf, lateral ulnar fossa; mc, metacarpal; mclr, lateral ridge of metacarpal I; mdcr, medial distal crest of humerus; med c, medial (tibial) condyle of femur; mt, metatarsal; ncs, neurocentral suture; of, olecranon fossa; pah, proximal articular surface of the humerus head; parap, parapophysis; part, pubic articular surface of ischium; pc, pollex claw; pcpl, posterior centroparapophyseal lamina; ph, phalanx; piid, posterior iliac indentation; pip, posterior iliac process; postz, postzygapophysis; pnf, pneumatic fossa; ppdl, paradiapophyseal lamina; pped, pubic peduncle; pr ant, anterior process of rib shaft; prdl, prezygodiapophyseal lamina; prez, prezygapophysis; pu, pubis; ra, radius; rug, rugosity; Sa, sacral vertebra; scap, scapula; sg, scapular glenoid; spdl, spinodiapophyseal lamina; spol, spinopostzygapophyseal lamina; sta, articular surface of coracoid with sternal apparatus; ti, tibia; tib, tibial articular surface of astragalus; tr pr, transverse process; tub, costal tuberculum; ul, ulna; un, ungual phalanx; vc, vertebral condyle; vco, vertebral cotyle*

Introduction

The remains of sauropod dinosaurs are abundant in terrestrial environments of the Late Jurassic to Late Cretaceous (Holtz et al. 2004; Weishampel et al. 2004), but articulated skeletons belong mostly to adult specimens. With a few exceptions (Gilmore 1925; Martin et al. 1994; Lehman and Coulson 2002) remains of early juvenile sauropods are restricted to isolated bones (Carpenter and McIntosh 1994; Foster 2005). Growth rates in sauropod dinosaurs have been studied based on histological data (Curry 1999; Sander 1999; Curry Rogers 2000; Sander 2000; Erickson et al. 2001; Sander and Tückmantel 2003). However, the knowledge about their ontogenetic changes is still limited, even in common taxa from the Late Jurassic Morrison Formation of North America, such as *Apatosaurus*, *Camarasaurus*, and *Diplodocus* (Curtice et al. 1996; Wilhite 1999; Bonnan 2001; Ikejiri 2003; Bonnan 2004; Ikejiri 2004a,b; Foster 2005; Wilhite 2005). The overall length of limb bones is thought to increase isometrically during ontogeny in those Morrison sauropods (Wilhite and Curtice 1998; Wilhite 1999; Bonnan 2001, 2004; Ikejiri et al. 2005b; Wilhite 2005) and the Early Cretaceous *Venenosaurus* (Tidwell and Wilhite 2005). *Camarasaurus* shows isometric growth in the humerus, radius and ulna, whereas the tibia exhibits a negative allometric growth relative to femoral length (Ikejiri 2004a,b). These studies are mainly based on long bones of late juvenile, subadult and adult individuals. Very little data are used from hatchling and early juvenile individuals (Carpenter and McIntosh 1994), so that the degree of proportional changes is still unclear in the early ontogenetic stage of sauropods.

The discovery of a nearly complete postcranial skeleton of an early juvenile sauropod at the Howe Stephens Quarry in Big Horn County, north central Wyoming (Figure 1) therefore is extraordinary. At the site, numerous dinosaur skeletons and tree trunks of

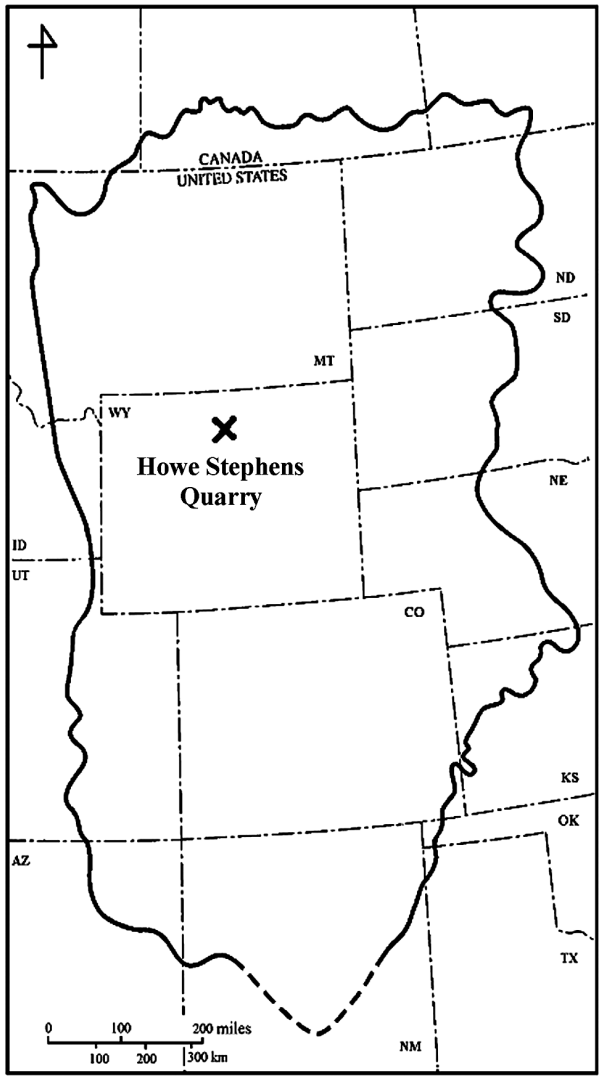

Figure 1. Geographic extent of the Morrison Formation with the locality of the Howe Stephens Quarry in northern Wyoming starred. Map modified from Turner and Peterson (1999) and Ikejiri (2005).

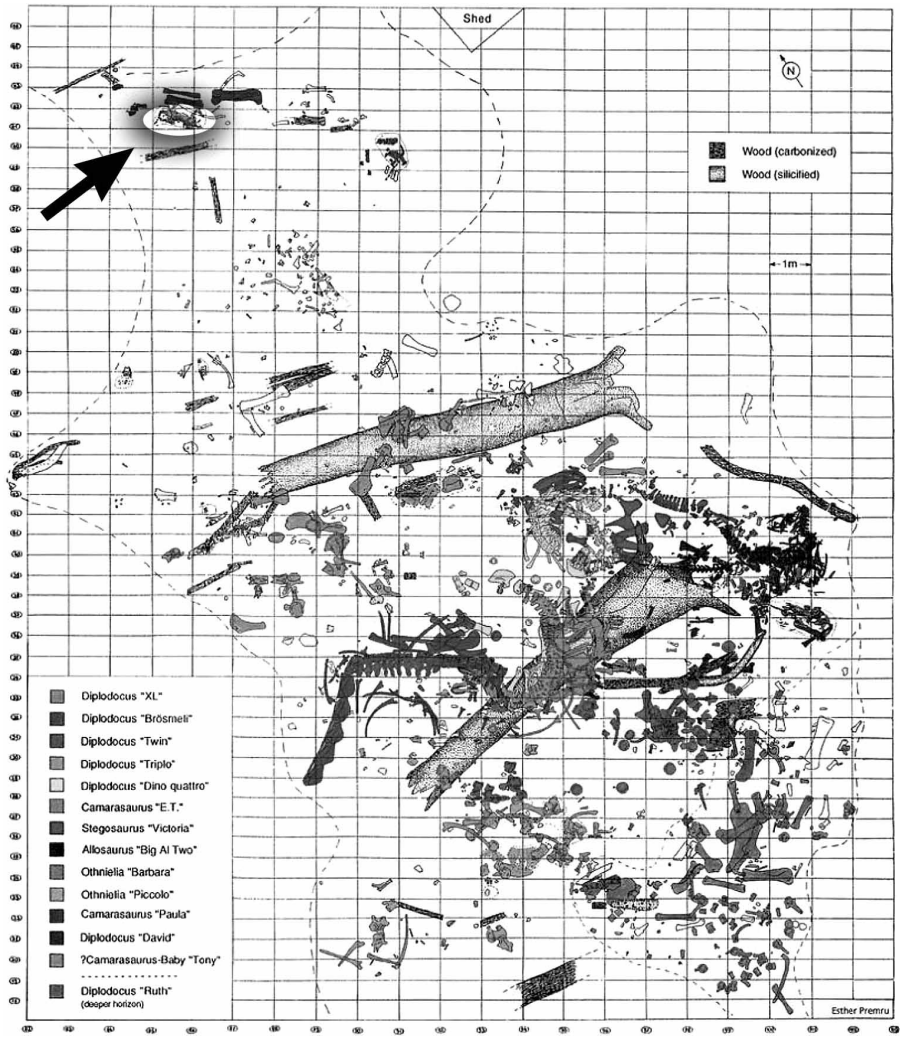

Figure 2. General site map of the Howe Stephens Quarry in Big Horn County, Wyoming during 1992 to 2001, with encircled area indicating the early juvenile diplodocid skeleton SMA 0009. Note that SMA 0009 was preliminary determined as '*Camarasaurus*-baby Toni.' This map was prepared by Esther Premru, © Sauriermuseum Aathal, Switzerland.

Araucaria have been found. In 1999, a juvenile sauropod skeleton was discovered near large limb bones of a diplodocid located near the northern edge of the quarry, (Figure 2). In honour of its discoverer Toni Fürst, the specimen was informally named 'Toni'. First assumed to belong to the hypsilophodontid *Othnielia*, the remains soon turned out to be a fairly complete, articulated skeleton of a small sauropod. The whole skeleton was transported to SMA and given an official collection number SMA 0009. After a temporary exhibition at the museum, the specimen was sent to the Black Hills Institute (BHI) in South Dakota for further preparation in 2004. Some additional, isolated bones of the tail were exposed from the matrix. A number of casts were produced from the skeleton and are now accessible for study at some other non-profit institutions (e.g., DMNH 53198). From spring 2005, the original skeleton SMA 0009 is on display in the Sauriermuseum Aathal in Switzerland.

The shoulder height of SMA 0009 is approximately 0.67 m, and the total body length is estimated to be less than 2 m. The overall body size of the juvenile sauropod is remarkably small when compared to fully-grown diplodocids. For example, an adult *Apatosaurus louisae* (CM 3018) reaches 2.91 m in shoulder height and over 18 m in body length. Besides such small body size, a number of morphological features (e.g., degree of fusion of vertebral elements) and histological data indicate that SMA 0009 is an early juvenile. In the axial skeleton of SMA 0009, large fossae enclosed by laminae and perforated by pneumatic foramina are evidence of vertebral pneumaticity (Wedel et al. 2000a; Wedel 2003a; O'Connor 2006). This makes statements about the process of pneumatisation in this skeleton possible. The completeness of the skeleton SMA 0009 provides significant information for better understanding relative growth, development of pneumatic spaces in the axial skeleton, and taxonomy of diplodocids (Ikejiri et al. 2005a).

Geological and historical framework

General geology

Lithologically, the Morrison Formation is variable, representing a 1.5 km^2 sedimentary sheet and extending 1500 km from north (southern Alberta) to south (southern New Mexico) and 1000 km from east (central Nebraska and South Dakota) to west (eastern Idaho to central Utah). Major fossiliferous outcrops are present in Arizona, Colorado, Montana, New Mexico, and Oklahoma, Utah, Wyoming (Russell 1989). The early major paleontological sites of the Morrison have been known since 1877 in Wyoming and Colorado (Ostrom and McIntosh 1966; Breithaupt 1998). Since that time, tens of thousands of fossils and hundreds of partial and nearly complete skeletons have been recovered for institutions throughout the world. Over 125 years of extensive collections, including plants (i.e., pollens, algae, leaves, grasses, and tree), invertebrates (i.e., snails, and ostracods) and vertebrates (i.e., fishes, turtles, lizards, crocodilians, pterosaurs, dinosaurs, and mammals) were used to reconstruct the paleoecosystem of the Rocky Mountain region during the Late Jurassic (Chure et al. 1998).

Vertical thickness of fluvial, lacustrine, and aeolian sediments is approximately 65 to 70 m in the Morrison Formation of the eastern Bighorn Basin of Wyoming (Swierc and Johnson 1996). This unit is underlain by the primarily marine, Jurassic Sundance Formation and overlain by the terrestrial, Early Cretaceous Cloverly Formation. The Morrison Formation within the eastern part of the Bighorn Basin was deposited on a low relief floodplain over the course of seven million years during the latest Jurassic (Swierc and Johnson 1996). Stratigraphically, SMA 0009 was found slightly above the primary producing layer of the original Howe Quarry (Figure 3), and is inferred to be approximately 145 million years old (Swierc and Johnson 1996). However, stratigraphic work by Turner and Peterson (1999) and current work by Jacques Ayer (Figure 3) indicate that the Howe Ranch quarries may be slightly older in age. SMA 0009 was embedded in a fine-grained, white, cross bedded sandstone, associated with plant material (*Araucaria* cones and numerous cone scales). This layer is approximately 35 m above above the limit between non-marine and marine sediments, which may form the contact to the underlying Sundance Formation and about 30 meters below the overlying Cloverly Formation (Figure 3).

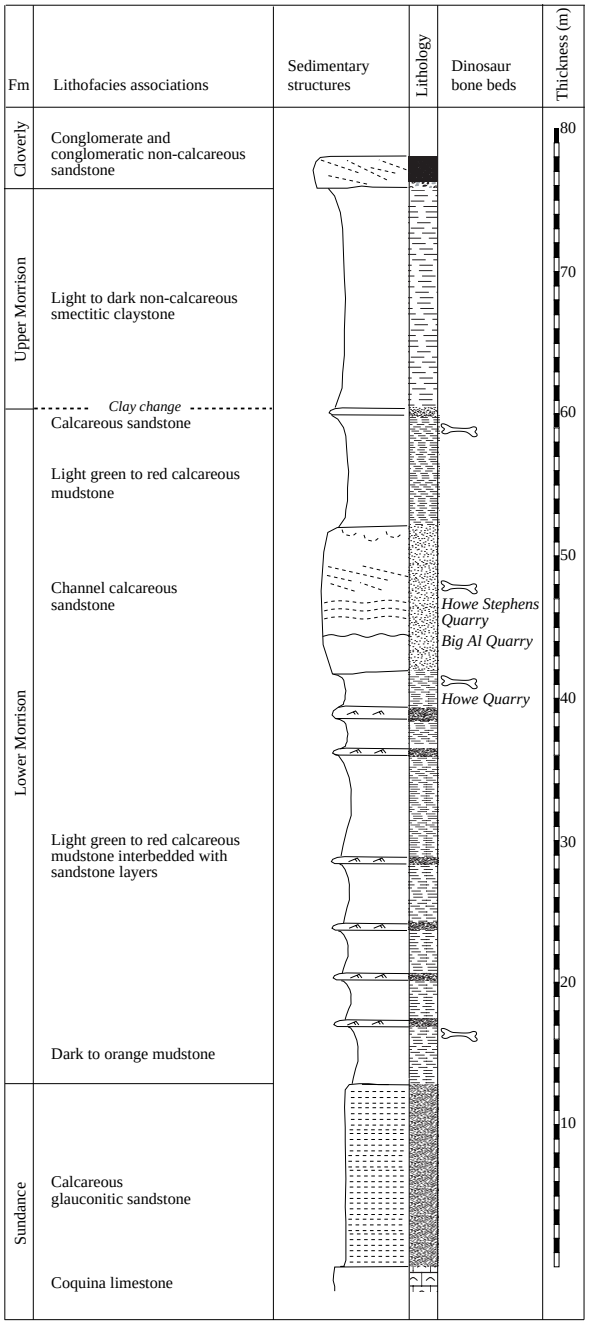

Figure 3. Composite stratigraphic column of the Morrison Formation in Bighorn County, Wyoming, showing position of Howe Stephens Quarry and of three other dinosaur bone beds. The limits between stratigraphic units are not clearly identified. © and production Jacques Ayer.

History of dinosaur collecting in this area

While collecting in the Lower Cretaceous rocks of the Bighorn Basin for New York's American Museum of Natural History in 1932, Barnum Brown was notified of the existence of large bones on the ranch of Mr. Barker Howe. A preliminary reconnaissance of the site revealed an area that promised to have an extremely fossiliferous quarry. Brown returned to the site outside of Shell, Wyoming in 1934 with a field crew from the American Museum of Natural History. Although only two sauropod skeletons were initially uncovered, later that summer a veritable, disarticulated herd had been discovered. Skeletal remains were crisscrossed and interlocked in a confusing almost inextricable manner in a clay unit beneath a relatively

thick sandstone layer (Bird 1985; Breithaupt 1997). For two months, bones were exposed, mapped and viewed by thousands of visitors from around the world. After being mapped and photographed, the specimens were painstakingly removed from the quarry. Over 30 metric tons of bones were collected from the Howe Quarry. Roughly six months after the quarry was opened, a total of 144 boxes of fossils were collected and loaded on a train bound for New York (Brown 1935; Colbert 1968).

The Howe Quarry produced over 4,000 dinosaur remains. Recent work by Michelis (2002) indicates that the actual number of bones collected may have only been 1800, including 600 remains collected by Siber in 1990 and 1991 (Hans-Jakob Siber, personal communication, 2003). Measuring 14 × 20 m, the original Howe Quarry contained one of densest concentrations of Jurassic dinosaur bones ever found. The assemblage of dinosaur fossils represented at least 20 different individuals. The quarry was dominated by sauropods, such as diplodocids and *Camarasaurus*, as well as ornithischian *Camptosaurus*. According to Michelis (2002), earlier accounts of *Diplodocus* being present were in error. Only isolated shed teeth of the theropod *Allosaurus* were discovered in the quarry. Most dinosaur skeletal remains were disarticulated, but a number of bones showed some degree of association. The Howe Quarry represents an accumulation of desiccated carcass parts that were washed into a small depression during a time of seasonal flooding (Breithaupt 1997). In addition to bones and teeth, footprints, skin impressions, and gastroliths have also been found in the Howe Quarry (Brown 1935; Ayer 2000).

In 1990, Siber & Siber, Inc. reopened the Howe Quarry with plans to uncover more dinosaur bones for SMA. The original Howe Quarry was expanded and produced additional material (Ayer 2000). However, it was not long until the bones of this fossiliferous lens in the Morrison Formation 'played out.' The Swiss collectors decided to expanded their operations laterally with hopes of finding the Howe Quarry bone layer elsewhere. In 1991, approximately 300 m to the north of the Howe Quarry, the team hit sauropod bones slightly above the level of the Howe Quarry. As excavation of these bones ensued in August, the collectors encountered some theropod vertebrae slightly above the sauropod remains. Careful excavation revealed not a random accumulation of disarticulated bones (as has been found at the Howe Quarry), but a single, nearly complete articulated skeleton of this *Allosaurus* (MOR 693). This fairly complete *Allosaurus*, with numerous pathologic bones (Hanna 2002), indicates the potential for important new discoveries to be made in areas of historic exploration in Wyoming (Breithaupt 2001).

The Siber team continued collecting in this area and reached the Howe Stephens quarry, which is located about 500 m southwest to the Howe Quarry. Over the next decade, they uncovered beautifully preserved and often partially articulated skeletons (Figure 3) of various Late Jurassic dinosaurs (e.g., *Allosaurus*, *Stegosaurus*, and *Camarasaurus*) currently on display in Aathal. In 1999, Austrian palaeontologist Toni Fürst joined the Siber dig team, and discovered the first bones of SMA 0009 while excavating the limb bones of a large diplodocids in the northern part of the Howe Stephens Quarry.

Preservation

SMA 0009 is an articulated partial skeleton on a matrix slab (Figure 4). The skeleton is partially broken and crossed by some fractures. Openings are filled with sediment matrix. During preparation, fractures in the bones were glued and small missing parts were remodelled with resin materials and painted. Cranial and mandibular elements, as well as the anterior cervical and distal caudal vertebrae are missing. The mid-cervical to mid-caudal vertebrae and most appendicular bones are articulated. Most presacral vertebrae are slightly distorted and dorsoventrally compressed. The sacral and caudal vertebrae and the appendicular bones are lateromedially compressed.

SMA 0009 has a total of 17 articulated presacral vertebrae, including eight posterior cervical (Cep-1 to Cep-8) and nine dorsal vertebrae (Do-1 to Do-9; Figure 4B). Cep-1 is exposed on its left side, being the only presacral vertebra where the neural spine is exposed laterally. The other presacral vertebrae are exposed in left ventrolateral view. The last cervical vertebra (Cep-8) is badly damaged. The last presacral vertebra Do-9 is tilted 90° with respect to the vertebral axis and strongly lateromedially compressed. In Cep-3, 4 and 6, the right cervical ribs are preserved *in situ* and exposed in ventromedial view. The dorsomedial surface of a broken cervical rib is visible beneath Cep-4. The remains of 13 dorsal ribs are spread along the presacral vertebrae over the slab and exposed either in anterior or posterior view.

The remains of the sacral and caudal vertebrae lie posteriorly adjacent to Do-9 and perpendicular to the other presacral vertebrae. All sacral and caudal vertebrae can be examined in left lateral view. Only a fragmentary part of the vertebral centrum of Sa-1 is visible in left lateral view, and from Sa-2 and Sa-3 only the neural arches with the postzygapophyses and sacral ribs are exposed. Sa-4 and Sa-5 have complete neural spines with the dorsal half of the neural arch and the sacral ribs. The unfused sacral ribs are broken away. Sa-2 to Sa-5 lie dorsally to the left ilium.

Twenty caudal vertebrae are preserved in SMA 0009, including 10 articulated anteriormost caudal (Ca-1 to Ca-10), six semi-articulated mid-caudal, and four isolated mid- or posterior caudal vertebrae (Ca-A to Ca-J) (Figure 4B). Two fragmentary chevrons from

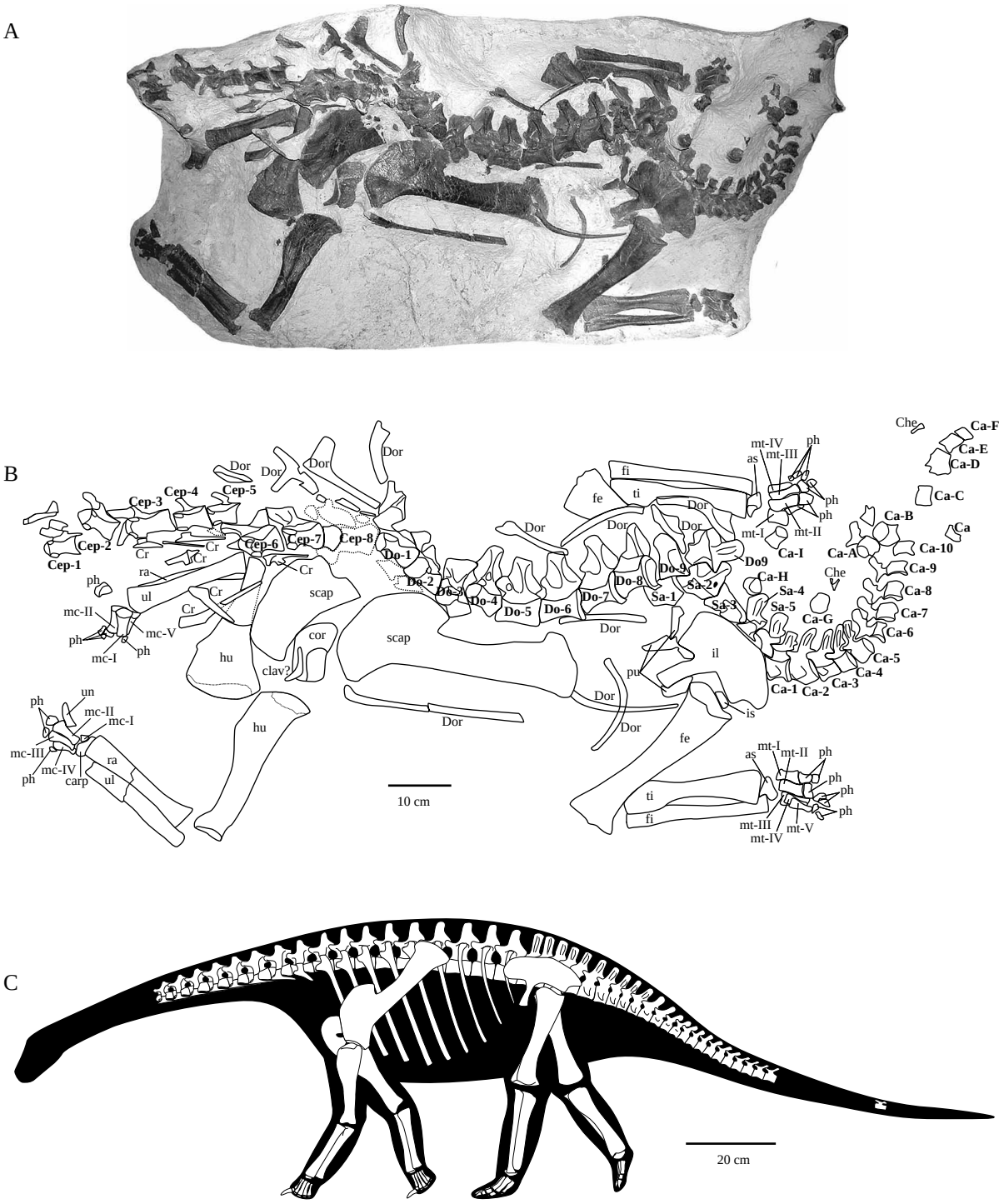

Figure 4. Skeleton of early juvenile diplodocid SMA 0009. (A) Photograph of the specimen. (B) Overview drawing of the skeletal remains exposed on the slab. For anatomical abbreviations, see text. (C) Reconstruction of the specimen.

the tail base are preserved, one exposed in left lateral view dorsally to Ca-6, and the other visible as a fragment dorsally to Ca-E.

The left scapula and coracoid are preserved in lateral view, with the posterior edge of the glenoid region of the left scapula being broken away. The medial surface of the ventral part of the right scapula is visible. The right coracoid was removed from matrix. Its scapular articular margin is strongly compressed, and the bone is distorted. At the lateral surface of the left coracoid and adjacent to its glenoid surface lies a small arcuate bone that might represent a clavicle. The left humerus, ulna, radius, and manus are articulated, with the humerus being angled for about 90° to the antebrachium and manus. The left humerus is exposed in posterior view, the left antebrachium and manus in anterolateral view. The proximal half of the right humerus is exposed posterolaterally, the rest

is covered by matrix and Cep-6. The anterolateral surface of the right ulna and the partial anterior surface of the right radius are visible. The right manus exposes the medial surface of metacarpals I, II and V.

The left ilium is preserved in lateral view, with its anterior margin being broken away. Plate-like fragmentary remains of the left pubis lie anteriorly adjacent to the left ilium. The iliac articular surface of the ischium is visible between the proximal end of the femur and the ischiac articular surface of the ilium. The left femur shows its anterolateral surface. The left crus and pes are exposed in posterior view. Only a distal part of the right femur is exposed in lateral view. Both the left and right femora are angled about 45° relative to the metatarsals. The posterior surfaces of the right tibia, fibula and pes are uncovered.

Taphonomy

The excellent preservation of SMA 0009 corresponds to weathering stages 0 or 1 (Behrensmeyer 1978) and indicates rapid burial by fluvial sediments near a river channel. The completeness and articulation of the skeleton indicate that the carcass was not transported very far from where the animal expired, representing essentially an autochthonous deposit. SMA 0009 does not show a death pose due to an opisthotonic body position, which is contrast to the fairly complete articulated skeleton of a late juvenile *Camarasaurus lentus* (CM 11338) from the Dinosaur National Monument in eastern Utah. The carcass of SMA 0009 seems to have been quickly embedded in the well-sorted fine-grained sandstone. The skull, anterior cervical, and posterior caudal vertebrae were not engulfed as quickly as the rest of the skeleton. They remained exposed long enough for the soft tissue to decay and to become disassociated from the rest of the skeleton. There is no strong evidence of scavenging events (e.g., shed teeth of carnivores, bite marks) associated with SMA 0009. In addition, close inspection of the bones shows no evidence of beetle or other invertebrate borings on the elements, as has been suggesting for other Late Jurassic carcass' found in the area (Laws et al. 1996; Hasiotis et al. 1999).

Description

Axial skeleton

Cervical vertebrae. The lack of anterior cervical vertebrae and the ventrolateral exposure of the vertebrae in SMA 0009 make it difficult to determine the exact count of presacral vertebrae with certainty. The preserved cervical vertebrae are numbered subsequently as posterior cervical vertebra Cep-1 to Cep-8 (Figure 4B). The position of the parapophyses in the cervical and the dorsal vertebrae is identical to that of *Barosaurus lentus* (McIntosh 2005). Cep-8 is considerably damaged and allows identifying either as last cervical or first dorsal vertebra. On the basis of the position of the parapophyses, which are placed on the lateral surface of the centrum, the next posteriorly adjacent vertebra is the first dorsal rather than the last cervical or second dorsal vertebra. Thus, we interpret the presacral vertebral column to consist of nine posteriormost cervical and nine dorsal vertebrae (Figure 4C).

The centra of the cervical vertebrae are opisthocoelous with a hemispherical anterior vertebral condyle surrounded by a flat and slightly roughened rim (Figure 5A,B). The relation between the overall length and transverse width of the centrum, (Elongation Index EI, sensu Upchurch 1998), ranges from 1.5 (Cep-6) to 1.9 (Cep-3), with a decrease of the EI posteriorly (Table I). There is a remarkable increase in length of the centrum between Cep-1 and Cep-2.

In ventral view, the centra of the cervical vertebrae are hourglass-shaped with a median constriction of one-fourth of their posterior width. The median two-thirds of the ventral surface are concave and bear a faint median crest (Figure 5A,B). Anteriorly and posteriorly, the ventral surfaces of the vertebral centra are covered with delicate, longitudinally oriented striae. The lateroventral margins of the centra are sharp in Cep-1 to Cep-5 and slightly broader and weaker in Cep-6 to Cep-8.

In all the cervical vertebrae, the parapophyses are located posteriorly adjacent to the vertebral condyle anteroventrally on the centrum. The parapophyses are longitudinally oval in outline and ventrolaterally directed, indicating that the capitulum is directed lateroventrally to the vertebral centrum. A posterior centroparapophyseal lamina forms the lateroventral margin of the vertebral centrum in the shape of a thin crest. The lateral surface of the vertebral centra from Cep-1 to Cep-7 bears a longitudinally oval-shaped pneumatic fossa divided into an anterior third and posterior two-thirds. The latter is covered by an irregular pitted texture, which decreases in depth posteriorly. The anterior and posterior pneumatic fossa both are perforated by a median pneumatic foramen. The size of the pneumatic fossae relative to their vertebral centra is consistent throughout all the cervical vertebrae in SMA 0009.

The neurocentral suture is visible in all preserved cervical vertebrae as an anteroposteriorly straight line. The diapophysis is directed anterolaterally. A broad, weakly concave prezygodiapophyseal lamina passes from the diapophysis to the prezygapophysis. The postzygodiapophyseal lamina bends posteromedially to reach the postzygapophysis from the diapophysis. From the internally directed, medial surface of the diapophysis the anterior centrodiapophyseal lamina descends anteriorly, and the posterior centrodiapophyseal lamina extends to the neurocentral suture. The rib articular surface of the diapophysis is slightly depressed between these two laminae. A shallow

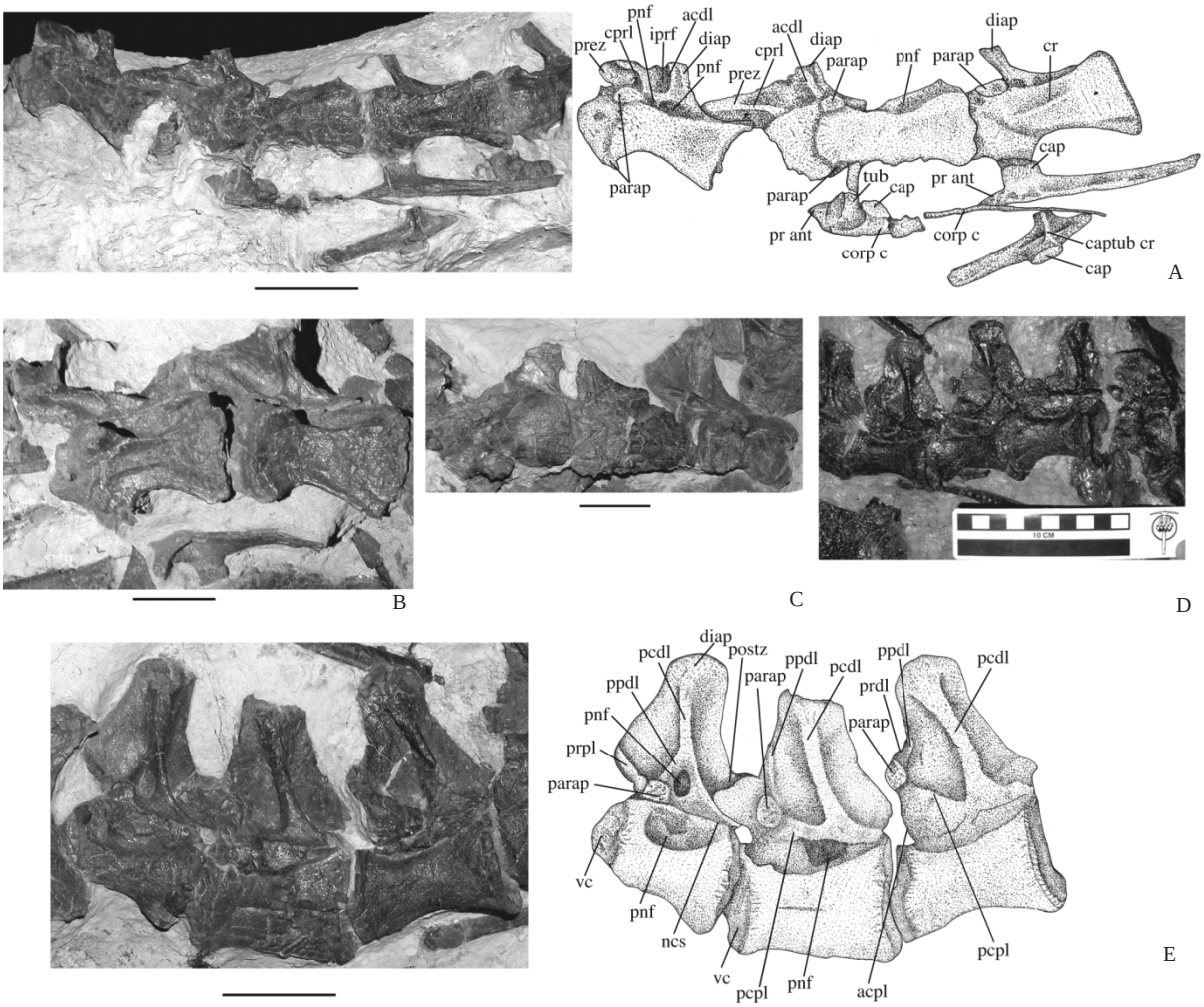

Figure 5. Presacral vertebrae of early juvenile diplodocid SMA 0009. (A) Photograph (left) and drawing (right) of Cep-2 to 4 in ventral aspect. (B) Photograph of Cep-6 and 7 in left ventrolateral view. (C) Photograph of cervicodorsal transition with presumed Do-1 to 3 in left ventrolateral aspect. (D) Photograph of posterior dorsal vertebrae (Do-7 to 9) in left lateral aspect. (E) Photograph (left) and drawing (right) of Do-4 to 6 in left ventrolateral aspect. Scale bar is 3 cm. For abbreviations, see text.

infradiapophyseal and infrapostzygapophyseal pneumatic fossa are visible in lateral view (Figure 5A,B).

The prezygapophysis is exposed in Cep-1 to Cep-3 and Cep-6 to Cep-7, where it is anteriorly elongate relative to the centrum length (Figure 5A,B), and connected by a centroprezygapophyseal lamina to the anterodorsal margin of the centrum (Figure 5A,B). The centroprezygapophyseal lamina is broader in Cep-6 to Cep-7 than in Cep-1 to Cep-3. In Cep-6 to Cep-7, the centroprezygapophyseal lamina directs about 50° anterodorsally from the horizontal plane. The space between the centroprezygapophyseal and the anterior centrodiapophyseal lamina is hollowed out by a prezygapophyseal pneumatic foramen that penetrates the diapophysis anteriorly.

The one preserved neural spine of Cep-1 tapers from ventrally to dorsally (Figure 4B). Its height is approximately one-third of the overall vertebral height, and the dorsal margin is strongly convex. Its anterior and posterior margins are weakly concave. The lateral surface of the neural spine is in its dorsal third covered with delicate, longitudinally directed crests.

Cervical ribs. The cervical ribs are not fused with their respective parapophyses and diapophyses in SMA 0009. The single complete, articulated cervical rib of Cep-3 is as long as 1.6 vertebral segments (Figures 4A and 5A). The shafts of the cervical ribs project posteriorly and taper in the posterior half to thin rods. The anterior process of the rib is broadened and ends in a narrow rounding approximately as long as the capitulum (Figure 5A,B).

In dorsal aspect, the rib shafts are anteriorly and posteriorly to the capitulum depressed (Figure 5A). The capitulum and tuberculum are connected by a lamina, which divides the trough transversely (Figure 6A,B). In the cervical rib lying ventrally to Cep-4, another lamina, which is half as high as the

Table I. Measurements of the juvenile diplodocid skeleton (SMA 0009). All measurements are in mm. ( ) = incomplete measurement. For anatomical abbreviations, see text.

	CL	WC	HC	EI	WD	LA	HA	LS	HNS
Cep-1	33.0	19.9	?	1.67	?	?	?	9.6	15.2
Cep-2	42.1	23.6	30.5	1.78	?	?	?	?	?
Cep-3	42.7	23.1	?	1.85	21.5	?	?	?	?
Cep-4	41.4	23.2	?	1.78	21.9	?	?	?	?
Cep-5	?	22.9	?		22.1	?	?	?	?
Cep-6	41.7	27.2	14.8	1.53	23.3	?	?	?	?
Cep-7	46.2	28.5	15.3	1.62	24.6	?	?	?	?
Cep-8	?	?	?	?	?	?	?	?	?
Do-1	48.3	23.6	?	2.04	?	?	?	?	?
Do-2	46.2	?	?		?	?	?	?	?
Do-3	41.0	30.2	?	1.36	?	?	?	?	?
Do-4	46.5	29.5	?	1.58	43.2	26.4	?	?	?
Do-5	51.0	23.9	?	2.13	47.8	30.1	?	?	?
Do-6	49.7	34.8	21.7	1.43	62.4	35.5	?	?	?
Do-7	51.2	36.8	?	1.39	64.7	?	?	?	?
Do-8	48.6	38.0	?	1.28	64.9	?	?	?	?
Do-9	?	38.0	?		63.1	?	?	?	?
Sa-1	?	?	?			29.8	14.9	18.4	41.1
Sa-2	?	?	?			28.6	?	18.2	40.8
Sa-3	?	?	?			?	?	?	?
Sa-4	?	?	?			?	23.3	18.9	38.2
Sa-5	?	?	?			?	24.4	19.6	35.1
Ca-1	21.0					20.2	18.4	15.3	?
Ca-2	14.3	?	23.0			15.7	22.9	14.7	35.4
Ca-3	25.0	?	25.1			12.2	18.7	17.1	37.4
Ca-4	18.7	?	24.3			12.3	16.4	14.6	39.6
Ca-5	19.6	?	21.8			11.8	14.7	10.5	32.6
Ca-6	21.3	?	68.2			11.4	15.9	15.2	32.4
Ca-7	19.1	?	28.3			6.9	?	11.4	22.5
Ca-8	18.6	?	24.6			5.2	?	15.2	22.7
Ca-9	14.8	?	22.7			?	?	7.7	24.5
Ca-10	15.1	?	?			5.2	?	?	?
Ca-A	25.4	26.0	20.2			?	?	?	?
Ca-B	24.3	11.8	16.8			?	?	?	?
Ca-C	23.6	25.2	15.8			?	?	?	?
Ca-D	22.4	?	22.2			?	?	?	?
Ca-E	21.3	?				?	?	?	?
Ca-F	21.1	?	17.9			?	?	?	?

	GL	PW	LW	DW	Ratio
Lt hu	181.6	83.0	34.1	41.7	hu:fe = .81
Lt ul	(138.0)	28.8	16.5	28.7	ul:hu = .76
Rt ul	136.0	29.0	16.8	27.9	
Lt ra	134.1	26.2	21.1	31.2	ra:ul = .97
Lt mc-II	44.3	12.6	16.6	20.1	mc-II:ra = .33
Lt mc-III	45.3	22.4	10.2	15.2	mc-III:mc-II = 1.02
Lt mc-IV	42.2		8.7	13.2	mc-III:mc-IV = 1.07
Rt mc-IV	40.1				
Rt mc-V	31.0	21.2	9.8	12.9	mc-IV:mc-V = 1.29
Lt un	34.0				
Lt fe	224.8	70.7	34.5	69.2	
Lt ti	186.5	46.0	22.5	49.5	ti:fe = .83
Rt ti	189.1				
Lt fi	192.4	(29.5)	15.8	19.4	ti:fi = .94
Rt fi	194.0				
Lt mt-I	32.0	14.6	9.4	20.7	mt-I:mt-III = .72
Rt mt-I	32.0				
Lt mt-II	40.5	18.4	16.7	19.5	mt-II:mt-III = .91
Rt mt-II	41.2				
Lt mt-III	44.5				mt-II:tibia = .22
Rt mt-III	44.0				
Lt mt-IV	36.0				mt-IV:mt-III = .81
Lt mt-V	31.0				mt-V:mt-III = .70

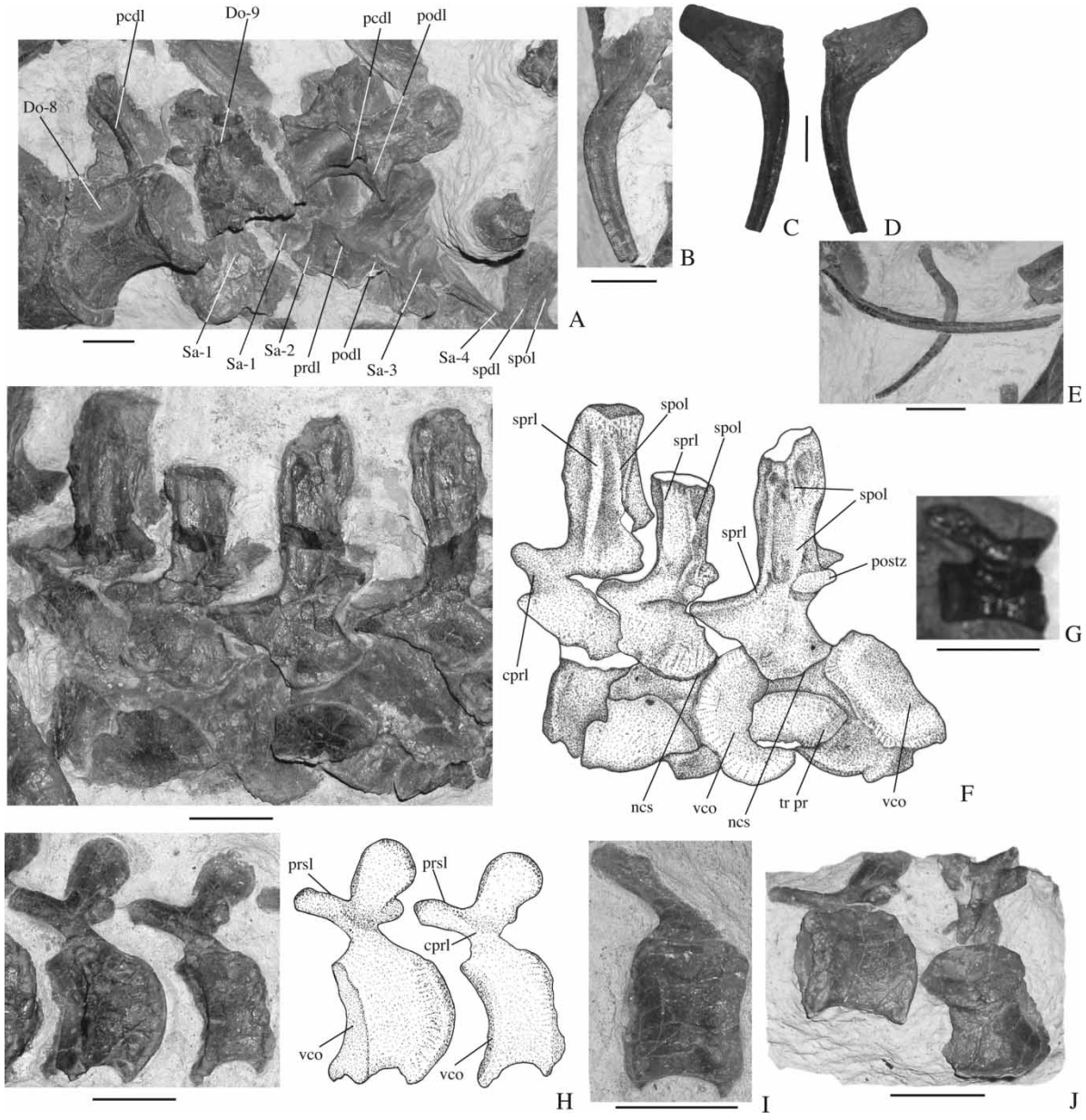

Figure 6. Detail photographs and drawings of dorsal ribs, sacral and caudal vertebrae of early juvenile diplodocid SMA 0009. (A) Photograph of Do-9 to Sa-4 in left lateral aspect. (B) Photograph of right anterior thoracic rib in lateral aspect. Photograph of right medial thoracic rib in (C) lateral and (D) medial aspects. (E) Photograph of left posterior dorsal ribs in lateral aspect. (F) Photograph (left) and drawing (right) of Sa-5 to Ca-2 in left lateral aspects. (G) Photograph of isolated mid-caudal vertebra in right lateral aspect. (H) photograph (left) and drawing (right) of Ca-8 to 9 in left lateral aspects. (I) Photograph of Ca-9 in left lateral aspect. (J) Photograph of Ca-A and B in left lateral aspects. Scale bar is 2 cm. For abbreviations, see text.

capitulum and has a concave dorsal margin, is visible crossing the transverse lamina perpendicularly (Figure 5A). The medial surface of the rib shaft is exposed in Cep-3. This surface bears posteriorly to the capitulum a longitudinally oval depression, and is distally to the depression strongly rugose (Figure 5A). The medial surface of the capitulum is perforated by a small circular foramen.

A. Vertebrae: CL, length of centrum without anterior condyle; **EI**, elongation index (*sensu* Upchurch 1998); **HA**, height of neural arch; **HC**, height of posterior cotyle (centrum); **HNS**, height of neural spine; **LA**, length of neural arch; **LS**, length of neural spine; **WC**, width of posterior cotyle (centrum); **WD**, transverse width of diapophysis. **B. Appendicular skeleton: DW**, width of distal end; **GL**, greatest length; **LW**, least width; **PW**, width of proximal end. **Left scapulocoracoid:** Scap GL. 311; scap length of shaft, 143; scap length of proximal (acromial) extremity, 122.3; scap proximal breadth, 148.1; scap least breadth of shaft, 38.5; scap distal breadth, 84.3; cor anteroposterior length, 76; cor dorsoventral height, 49, cor foramen diameter, 23. **Left ilium:** GL, 164; postacetabular length, 88; postacetabular height, 60.9; height of pubic peduncle, 67.7; transverse width of pubic peduncle, 67.7. **Limb bones**.

Dorsal vertebrae. The vertebral centra between Do-1 and Do-3 are strongly opisthocoelous. The degree of convexity on the anterior surface of the centra rapidly decreases from Do-4 to Do-5 (Figure 5C), but opisthocoelous centra are found up to Do-9. The anteriormost dorsal vertebra is slightly longer than Cep-7, and overall length of the dorsal centra increases in posterior direction. Do-7 has the longest centrum in the dorsal series. The EI value varies between 1,28 and 2.13, the largest value being reached in the possibly deformed Do-5 (Table I). In ventral view, the centra of Do-1 to Do-6 are hourglass-shaped (Figure 5C). In contrast to the cervical vertebrae, the centra of the dorsal vertebrae are ventrally smooth and rounded, and only their anterior and posterior margins are slightly roughened.

The parapophyses of Do-1 and Do-2 lie anteroventrally at the lateral surface of the centrum and send a large, rounded prezygoparapophyseal lamina in anterodorsal direction to the prezygapophysis. A large pneumatic fossa relative to overall size of the centrum is positioned posterodorsally to the parapophysis on the lateral surface of the centrum. In Do-3, the parapophysis is positioned in the anteromedial third of the lateral surface of the centrum, with the pneumatic fossa being positioned posteriorly adjacent to the parapophysis. In Do-4, the parapophysis lies anteriorly near the neurocentral suture, and a longitudinally oval-shaped pneumatic fossa with a median foramen is visible ventrally to the parapophysis (Figure 5C). The parapophysis of Do-5 is located on the transverse process slightly ventrally to the prezygodiapophyseal lamina, anteroventrally and medially to the diapophysis articular surface. The parapophysis of Do-3 to Do-7 exhibits a rounded outline of the prezygoparapophyseal lamina (Figure 5C–E). Posterior to Do-4, a paradiapophyseal lamina is present, ascending posterodorsally until the posterior centrodiapophyseal lamina. In Do-6 and Do-7, an anterior centroparapophyseal lamina is exposed, joining the parapophysis to the anterior margin of the centrum. A posterior centroparapophyseal lamina is exposed from Do-4 to Do-7. In Do-6 to Do-9 a pneumatic fossa at the lateral surface of the centrum is lacking.

The neural arch and centrum are unfused in all the dorsal vertebrae (Figure 5D,E). The transverse processes of the dorsal vertebrae (see above) are laterally directed and taper to half their medial length (Figure 5C). The prezygodiapophyseal lamina is constricted at the anterior margin of the transverse process. The postzygodiapophyseal lamina is placed on the weakly concave ventral margin of the transverse process. The lateral margin of the transverse process bears the rib articular surface and is rounded and broadened.

The ventral surface of the transverse process is separated into anterior and posterior halves by a bulging posterior centrodiapophyseal lamina (Figure 5D,E). The posterior centrodiapophyseal lamina runs at the ventral surface of the transverse process from its lateral margins straight medially to its base, where it turns posteroventrally to end dorsally to the neurocentral suture. Do-2 bears a transversely oval-shaped infradiapophyseal pneumatic fossa at the base of the transverse process (Figure 5C), enclosed by the paradiapophyseal and posterior centrodiapophyseal laminae.

Dorsal ribs. The longest of the preserved dorsal ribs, belonging most probably to Do-4 or 5, is as long as five vertebral segments. The shortest ribs, belonging to one of the posterior dorsal vertebrae, reach the length of 2.5 vertebral segments.

The anterior dorsal ribs are somewhat twisted, and their shafts are curved proximally and nearly straight distally. The rib head is flattened anteroposteriorly, and capitulum and tuberculum are separated from each other by a wide and slightly concave incision (Figure 6A–C). In the anteriormost dorsal ribs, the capitulum is approximately three times as long and broad as the tuberculum (Figure 4A). The anterior and posterior surfaces and the medial margin of capitulum and tuberculum are roughened. Between capitulum and tuberculum, the anterior surface of the rib is slightly depressed. From both capitulum and tuberculum, a rounded crest extends ventrally (Figure 6A,B), uniting at the proximal third of the rib shaft to form a rounded anterolateral margin of the rib. The rib shaft flattens after its proximal third in anteroposterior direction. The anterior and posterior surface of the rib shaft bears a shallow groove. The distal ends of the anterior dorsal ribs are broken away, but there seems to be a distal expansion of the rib shaft.

The posterior dorsal ribs are remarkably more slender than the anterior ribs (Figure 4A,B) and possess strongly curved shafts (Figure 6D). The rib shafts tends to be even more flattened than in the anterior dorsal ribs. In the capitulotubercular region, the rib corpus is lateromedially broadened and ends dorsally with a bowl-shaped capitulotubercular articular surface, surrounded by a rim of delicate striae. The medial surface of the rib shaft bears a deep groove (Figure 6D). In none of the ribs, pneumatic foramina are found.

Sacral vertebrae. The vertebral centra are unfused in Sa-1 and Sa-2 (Figure 6E). The neural arches of Sa-2 and Sa-3 are contiguous, but not completely fused. Sa-4 and Sa-5 possess unfused centra. The neurocentral suture of Sa-2 and Sa-3 is horizontal. The neural arch peduncle of Sa-2 and Sa-3 is one-third the height of the neural spine. A longitudinal

crest forms anteriorly the prezygodiapophyseal and posteriorly the postzygodiapophyseal lamina. Dorsal to the sacral ribs, the surface of the neural arch is slightly depressed in Sa-2 to 5. On the dorsal surface of the postzygapophysis of Sa 4 lies a pit with a lateromedially oval outline.

The neural spines of Sa-2, Sa-4 and Sa-5 have a slightly concave anterior and posterior margin. The dorsal margin is slightly convex, broadened and roughened (Figure 6E). In lateral view, the neural spines are slightly constricted at their base and reach approximately three-fourths of the length of the vertebral centrum. A broad spinopostzygapophyseal lamina ascends from the dorsal surface of the postzygapophysis over the posterior third of the lateral surface of the neural spine to its roughened dorsal part. A spinodiapophyseal lamina ascends from the sacral ribs to the middle of the neural spine (Figure 6E).

Caudal vertebrae. The centra of all caudal vertebrae possess a weakly concave anterior articular surface, whereas the posterior articular surface is planar with a weak depression in its medial third (Figure 6F–H). The anterior and posterior articular surface is surrounded by a bulging and rugose rim, which overhangs in lateral view the ventral surface of the centrum. In lateral view, the vertebral centra have a smooth, slightly concave lateral surface.

The centra of Ca-1 to Ca-6 reach in height 60% of their length and increase in height between Ca-7 and Ca-10 to become one-fourth higher than long. In the mid-caudal vertebrae (Ca-A to Ca-F) and the isolated caudal (Figure 6J), the centra become one-third longer than they are high (Figure 6I,J). In ventral view, the centra are hourglass-shaped with a maximum constriction of one-fourth of their posterior width (Figure 6I). The posterior margin of the ventral face of the centra forms a relatively small chevron facet (Figure 6I), which merges with the posterior articular surface of the centra.

Transverse processes are present in Ca-1 to Ca-7 (Figure 6F), including suturally connected caudal ribs to the vertebral centra in Ca-1 to Ca-3 and complete processes in Ca-4 to Ca-7. The transverse processes project laterally. Their anterior and posterior margins slightly converge in lateral direction so that the processes taper laterally for one-third of their medial length. The dorsal surface of the transverse processes is weakly roughened.

The neurocentral suture is a horizontal, serrated line in Ca-1 to Ca-10. Ca-1 to Ca-6 possess neural arch peduncles that are as high as the centrum. Posteriorly to Ca-6, the neural arch peduncles gradually decrease in height. The lateral surface of the neural arch peduncle is weakly concave. The prezygapophyses form long straight struts, and the articular surfaces are covered with the matrix. The lateral surface of the prezygapophyses is covered with longitudinally oriented striae. In Ca-1 to Ca-6, a rounded spinoprezygapophyseal lamina proceeds from the dorsal margin of the prezygapophysis to the lateral surface of the neural spine (Figure 6F), where this lamina meets the spinopostzygapophyseal lamina. A centroprezygapophyseal lamina is developed in Ca-1 to 10 and at least in Ca-A and B. The centroprezygapophyseal lamina extends from the anterior margin of the prezygapophysis strut ventrally to end dorsally adjacent to the neurocentral suture (Figure 6F,H). Postzygapophyses are visible in Ca-1 to Ca-10 and Ca-A and B, with an angle of ca. 50° to the horizontal plane. The postzygapophyses are positioned at a level dorsal to the prezygapophysis and consist only of their articular surface, attached to the lateral surface of the neural spine. In Ca-1 to Ca-7, the spinopostzygapophyseal lamina extends from the postzygapophyses over the ventral four-fifths of the lateral surface of the neural spine (Figure 6F).

In lateral view, the neural spines of Ca-1 to Ca-5 are slightly constricted at their base and anteroposteriorly widened in their dorsal two-thirds. The neural spines are dorsally directed and reach about 1.5 times the height of the centrum. The anterior, posterior and dorsal margins of the neural spines are slightly convex. The dorsal margin is broadened and weakly rugose. In its dorsal fifth, the lateral surface of the neural spines is broadened and roughened.

Terminal to Ca-5, the neural spines become more posterodorsally inclined and decrease in height to 80% of the height of the vertebral centra, in the medial caudal region even to half of the height of the centra (Figure 4A,B; Figure 6G–J). The dorsal margins of the neural spines in Ca-7 to the posterior caudal vertebrae are convex.

Chevrons. Two fragmentary chevrons possess a body that divides into two lateral processes enclosing the haemal canal (Figure 4A,B). The dorsal part of the left lateral process is broken away, so that it is not visible if both processes unite dorsally to roof the haemal canal. In anterior view, the blade of the chevron tapers ventrally.

Appendicular skeleton

Scapula. The left scapula is remarkably large and longitudinally elongated relative to the overall body size (Figures 4 and 7). The scapular shaft is elongate and slender (Figure 8A). Its proximodistal length reaches about three times of the length of the proximal end. The dorsal and ventral margins of the scapular shaft are straight, and diverge distally to form the slightly expanded blade. The scapular blade ends with a convex distal margin, the anterior corner of which

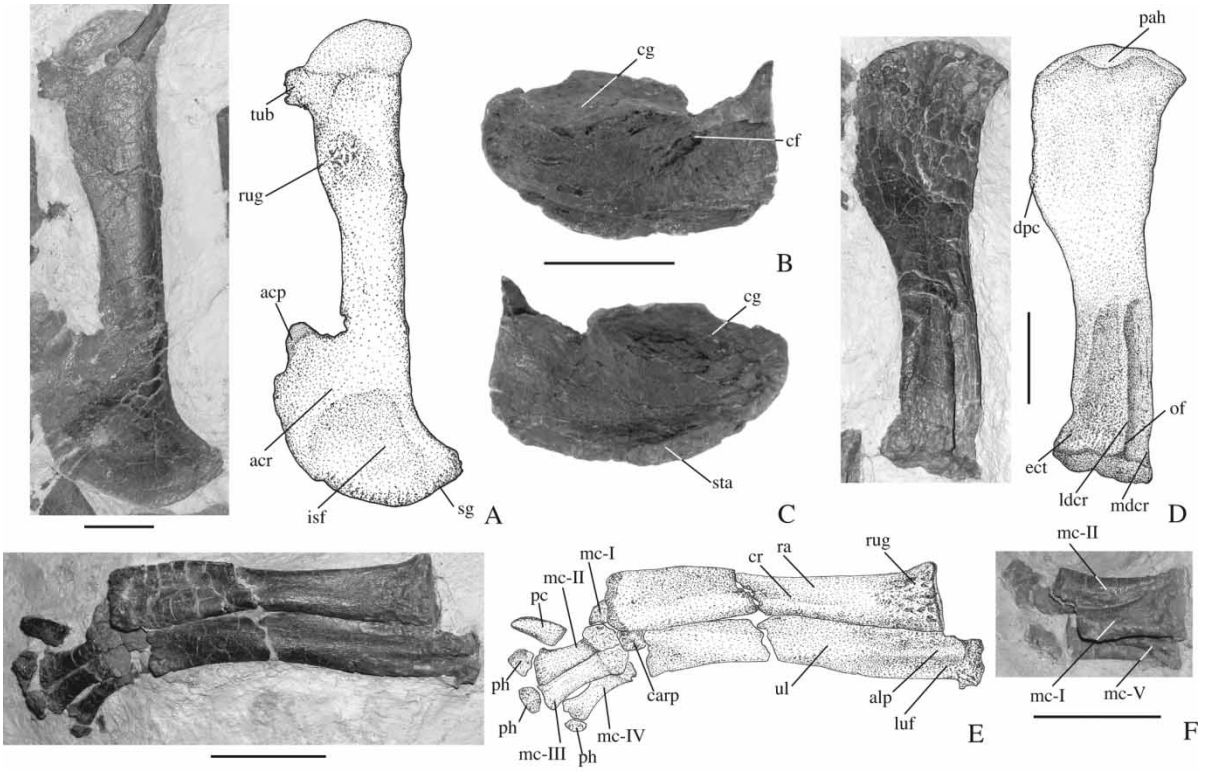

Figure 7. Photographs and drawing of shoulder girdle and forelimb of early juvenile diplodocid SMA 0009. (A) Photograph (left) and drawing (right) of left scapula in lateral aspect. Photograph of right coracoid in (B) lateral and (C) medial aspect. (D) Photograph (left) and drawing (right) of left humerus in anterolateral aspect. (E) Photograph (left) and drawing (right) of left radius, ulna and manus in anterior aspect. (F) Photograph of right manus in medial aspect. Scale bar is 5 cm. For abbreviations, see text.

bears a tuberosity (Figure 7A). The posterodorsal third of the lateral surface of the scapular shaft bears a circular rugosity consisting of small crests.

The acromial region of the scapula is expanded anteroposteriorly and twice as wide as the scapular shaft. The anterior margin of the proximal end is slightly convex and bears proximodistally directed striae, but the anterior acromion process is narrow with an anterodorsally pointed tip (Figure 7A). The scapular glenoid area is only exposed from laterally. The coracoid articular surface extends to the posteroventral fourth of the ventral scapular margin.

The lateral surface of the proximal end of the left scapula bears centrally a shallow infrascapular fossa,

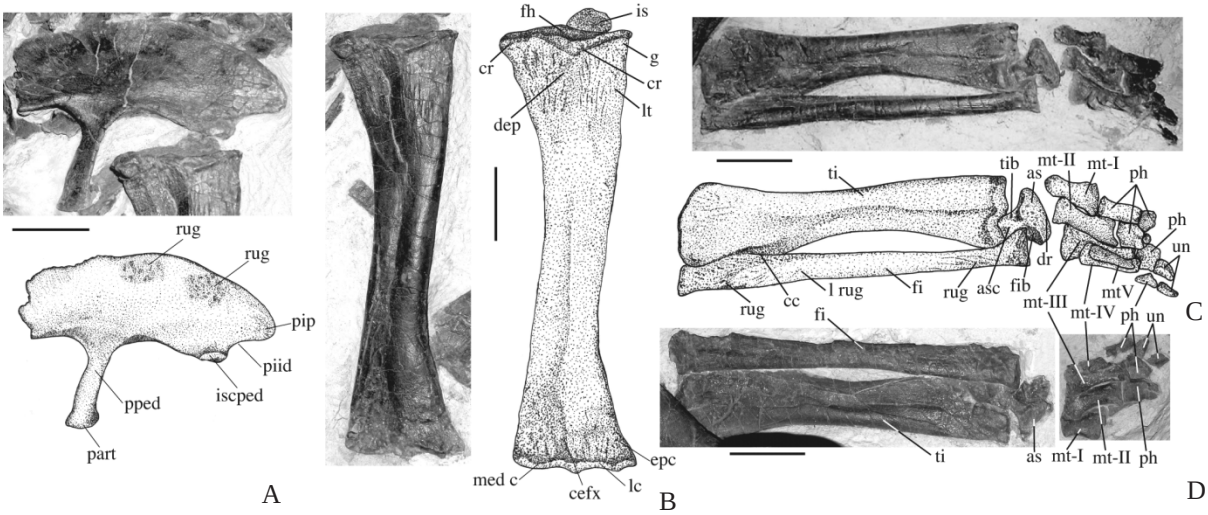

Figure 8. Photographs and drawing of elements of the pelvic girdle and hind limb of early juvenile diplodocid SMA 0009. (A) Photograph (above) and drawing (below) of left ilium in lateral aspect. (B) Photograph (left) and drawing (right) of left femur in posterolateral aspect. (C) Photograph (above) and drawing (middle) of left tibia, fibula, and pes in posterior aspect. (D) Photograph of right fibula, tibia, and pes in posterior aspect. Scale bar is 5 cm. For abbreviations, see text.

bounded anteriorly by a weak acromion ridge ascending anterodorsally to the anterior margin of the scapular head. The angle between the acromion ridge and the scapular shaft is about 100°. Posterior to the infrascapular fossa, the margin of the proximal end forms dorsally to the glenoid a rounded bulge. The visible medial surface of the proximal end of the right scapular is weakly concave (Figure 7A).

Coracoid. The coracoid is relatively small and its anterodorsal margin is convex in outline (Figure 4A), and unfused to the scapula. The scapular articular surface of the coracoid is articulated with the proximal end of the scapula and forms a dorsally pointing tip (Figure 7B,C). The longitudinally oval-shaped glenoid surface is relatively thick and comprises the posterior two-thirds of the proximal coracoid margin (Figure 7B). The glenoid forms a rounded V-shaped notch, and the articular surfaces of both the coracoid and scapula share about the same length. The dorsoventrally oval-shaped coracoid foramen is placed at the point of maximum concavity of the scapular articular margin and perforates the bone posteromedially (Figure 7B,C).

Clavicle. Adjacent to the glenoid surface of the lateral surface of the left coracoid lies a small curved bone, which could be interpreted from its size, morphology and position as a possible clavicle (Figure 4A,B). This arcuate element has a convex posterior and a strongly concave anterior margin and tapers to both ends. The supposed clavicle is half as long as the coracoid and its external surface is smooth. The bone lacks a bifurcate lateral margin present in the clavicles of *Diplodocus* (Hatcher 1901; Holland 1906) and *Apatosaurus* (Filla and Redman 1994), but resembles the latter in its curvature. Another possibility would be that this bone represents a furcula. In contrast to clavicles (Hatcher 1901; Holland 1906; Dong et al. 1983; Zhang et al. 1984; Sereno et al. 1999; Yates and Vasconcelos 2005), the latter element has not been found in any other sauropod, so that such a possibility is doubtful. Although overall shape would make also an assignment as gastralium possible (Claessens 2004), the position of the bone directly at the left coracoid makes this assignment less probable than its interpretation as clavicle.

Humerus. The left humerus is about 20% shorter than the left femur (Table I). The humerus possesses an anteroposteriorly compressed shaft that widens transversely. The uncompressed proximal end of the right humerus reaches three times of the width of the shaft (Figures 4A and 7D) and its lateral and medial margins are moderately expanded. The humeral head has a weakly convex margin that curves medially to the deltopectoral crest. The deltopectoral crest is visible posteriorly, diving anteroventrally into the sediment (Figure 7D). The crest occupies approximately 30% of the total length of the humerus. In proximal view, the humeral head bears a prominent rounded, posteriorly directed median tuber that slightly overhangs the posterior surface (Figures 4A and 7D). The lateral corner of the humeral head forms a short projection. Distally to the humeral head, the anteroproximal surface is roughened.

The ulnar and radial articular surfaces of the humerus are surrounded by a rim of delicate, proximodistally oriented striae and separated from each other by a shallow median groove. The ulnar articular surface is oval in outline with a longitudinally oriented long axis. The radial articular surface is one-fourth larger than the ulnar articular surface and transversely oriented. The separating median groove extends as olecranon fossa to the posterior surface of the distal humeral end. The posterior face of the distal humeral end is covered by coarse, vertically directed crests. The laterally positioned epicondyle is roughened (Figure 7D).

Ulna and radius. The left ulna is 3% longer than the left radius and is 75% of the humeral length (Table I). The mid-shaft diameter of the ulna and radius is roughly equal. The lateral margin of the ulna is slightly concave and the medial margin is slightly convex. In anterior view, the proximal end of the ulna possesses a prominent, roughened anterolateral process (Figure 7E). Slightly roughened vertical grooves extend from both laterally and medially to the anterolateral process over the proximal half of the ulnar shaft. The posterior surface of the distal end of the ulna bears a median rugosity and is slightly depressed. The anterior surface of the distal end is medially concave and roughened. The median depression is laterally separated from the rest of the surface by a rounded bulge (Figure 7E).

The left radius has a constricted shaft, which is in its proximal part half as wide as distally (Figure 7E). The lateral and medial margins of the radius are slightly concave. The radial head is transversely oval in outline and slightly depressed. The anteromedial surface of the proximal end of the radius bears a median rugosity with a rounded triangular outline. The radius shaft bears anteromedially a rounded and slightly roughened ridge. Distally, the anteromedial surface of the radius is slightly concave. The distal end of the radius has a roughened circumference.

Carpals. The left carpal I (Figure 7E) is preserved with its lateral half in proximal view. The carpal I is plate-like and transversely oval in outline. Its exposed

proximal surface is rugose, but no medial ridge can be recognized.

Metacarpals. The articulated left (Figure 7E) and right (Figure 7F) metacarpals I to V are arranged in a weak anteriorly convex arch. In the right manus, metacarpal I lies on the medial surface of metacarpals II and V. The left metacarpal II measures 33% of the greatest length of the radius and is slightly shorter than metacarpal III (Table I). In the left manus, the proximal end of metacarpal III is one-third narrower than that of the metacarpals II and IV (Figure 7E).

The metacarpal shafts comprise four-fifths of their total length and are transversely oval in cross-section. The proximal end of the metacarpals is anteroposteriorly elongated. The distal end is transversely expanded in relation to the shaft so that both articular surfaces have a long axis oriented perpendicular to each other. In proximal view, the articular surface of the left metacarpals I and II is rounded trapezoidal, and that of the left metacarpal III is rounded triangular with one tip pointing posteriorly (Figure 7E). All proximal articular surfaces are covered with a regular pattern of shallow pits and ridges. In anterior view, the proximal articular surface is medially depressed and slightly roughened. The distal end of the metacarpals is surrounded by fine, proximodistally directed striae.

Manual phalanges. Only fragmentary remains of the proximal phalanges are preserved (Figure 7E,F). These phalanges are stout and wider than long. In the left manus, the proximal phalanx of digit II is box-shaped and 1.5 times as wide as it is high, with a rounded and trapezoidal, slightly medially depressed proximal articular surface. The proximal articular surface of the proximal phalanx of digit III is rounded rectangular and medially depressed. The proximal phalanx of digit IV is transversely oval in cross section.

The left ungual phalanx (pollex claw) lies medially to the position of metacarpal II (Figure 7E). The ungual phalanx is half as long as the left metacarpal III and reaches three-fourths of the length of the right metacarpal I (Table I). The ungual phalanx is transversely compressed and in lateral view is rounded triangular in outline, tapering from proximally to distally to a narrow rounding. Its dorsal margin is very weakly convex, but the ventral margin is nearly straight. The proximal articular surface of the ungual phalanx is rounded triangular with an anteriorly directed tip. The exposed medial surface of the ungual phalanx is crossed by a proximodistal, medial groove.

Ilium. The dorsoventral height of the iliac body is about the same as the pubic peduncle (Figure 8A). The dorsal margin of the ilium is weakly convex. The posterior margin of the iliac body forms a dorsal process and a ventral, rounded ischiac peduncle separated from each other by an indentation. The posterior dorsal process of the ilium is twice as long as the ischiac peduncle and overhangs the latter. The articular surface of the ischiac peduncle is directed posteroventrally (Figure 8A).

In lateral view, the iliac body is slightly concave medially. The dorsal half of the iliac body is covered by delicate vertical striae anterior to the pubic peduncle. In the medial third of the iliac body, there lies a rugosity, followed by another rugosity posteriorly (Figure 8A). The posterior half of the dorsal margin bears coarse crests, which are maximally developed at the posterodorsal iliac process.

The pubic peduncle is slender and elongate, and located in the anterior half of the iliac body. Its long axis is perpendicular to the long axis of the iliac body, and slightly anteroposteriorly twisted (Figure 9A). The pubic peduncle is 1.2 times the height of the iliac body and is weakly expanded distally. Anterior and posterior to the pubic peduncle, the ventral margin of the iliac body is slightly concave. The ventral pubic articular surface bears a rim of delicate striae.

Ischium and pubis. From the left ischium, only a longitudinally oval proximal articular surface is preserved, the rest being still in the matrix (Figure 4A,B; Figure 8A). Broken, plate-like remains of the left pubis are visible directly ventrally to the anterior part of the left ilium (Figure 4A,B), but they are too fragmentary to be described in detail.

Femur. The left femur (Figure 8B) has a straight shaft, with its distal end slightly bent posteriorly. The proximal and the distal ends are similar in transverse width and one-third wider than the minimum mid-shaft width.

The femoral head has a kidney-shaped articular surface with an indentation at its lateral surface. The femoral head is surrounded by a bulging rim of coarse, proximodistally oriented striae. The femoral head is proximally drawn out into an anteromedial and an anterolateral projection, from which each a rounded crest descends over the anterior surface of the proximal end of the femur. Both vertical crests enclose a medial shallow depression (Figure 8B), which might be the result of a moderate compaction of the bone. From this depression, vertical, coarse crests descend distally (Figure 8B). The lesser trochanter is not clearly exposed, but detectable in posterior view as a rounded, medially bulging crest (Figure 8B). The posterior surface of the lesser trochanter is roughened.

At the distal end, the lateral condyle is one-fourth larger than the medial condyle and has an anteromedially-posterolaterally oriented long axis. Both condyles

Figure 9. Photomicrograph of the histology of the anterolateral side of the femur of SMA 0009. The plane of section is perpendicular to the long axis of the femur, bone surface is at the top. Note the large size of the vascular canals and their irregular arrangement in the innermost cortex (arrow), the lack of primary osteons, and the plump and numerous osteocyte lacunae. Scale bar is 2 mm.

are separated only weakly from each other by a faint intercondylar sulcus and continue as bulges onto the anterolateral surface of the femur (Figure 8B). The lateral epicondyle is strongly roughened. In lateral view the femoral shaft bears a median groove that widens in distal direction until it ends between the bulges of the lateral and medial distal condyle (Figure 8B). The groove is at the distal femoral end strongly roughened. Proximally to the medial condyle, the anterolateral surface of the distal femoral end bears a vertically oval depression.

Tibia and fibula. The left tibia (Figure 8C) is 6% shorter than the left fibula and is 83% of the length of the left femur (Table I). The tibia has a strongly constricted shaft that is two-fifths of the proximal tibial width (Figure 8C,D). The shaft extends for the medial two-thirds of the greatest tibial length. The lateral margin of the tibia is weakly concave and the medial margin is strongly concave. The proximal end of the tibia is strongly expanded transversely and one-fourth wider than the distal tibial end. Both tibiae and fibulae are preserved in articulation, with the cnemial crest buried under the fibula (Figure 8C,D).

From the tibial head, a prominent bulge descends medially to the cnemial crest over the proximal third of the posterior surface. The posterior surface of the proximal end is medially to this bulge depressed and weakly roughened. Distal to the bulge, a faint median groove divides the tibial shaft into a lateral and a medial half, and descends to the posterior surface of the distal end (Figure 8C,D). The distal articular surface of the tibia is compressed. The astragalar articular surface is more prominent than the medial articular surface and forms a posterodorsally directed tuber with a slight medial depression. Proximally to the distal articular surface, the posterior surface of the distal end of the tibia is roughened.

The fibula has a straight shaft that tapers continuously proximally to distally (Figure 8C,D). The proximal end of the fibula is anteroposteriorly expanded and comprises the proximal fourth of the total length of the fibula. In posteromedial view, the proximal fibular end is concave. The posterolateral margin is broadened to form a rugosity with vertical little crests (Figure 8C). The distal end is at its articular surface expanded and surrounded by vertical striae. The distal articular surface is depressed and rounded rectangular in outline. At the lateral surface of the distal fibular end lies a circular, slightly roughened depression.

Astragalus. The astragalus is exposed in posterodorsal view (Figure 8C,D). The bone has a rounded triangular outline with a rounded projection pointing anterodorsally. The medial process of the astragalus is one-third longer than the anterior and lateral ones. The dorsal surface of the astragalus is crossed by a median longitudinal crest, laterally and medially to which lie each a depression. The lateral depression represents the astragalar surfaces for the fibula and is one-third smaller than the medial depression. The medial depression is the astragalar surface for the tibia and bears two tiny foramina (Figure 8C). The distal roller of the astragalus is slightly inflated (Figure 8C).

Metatarsals. The pes possesses five metatarsals (Figure 8C,D), of which metatarsal III is the longest (Table I). Metatarsal I has the widest lateromedial extension with a distal medial process that bends laterally to articulate with the medial surface of metatarsal II.

The proximal end of metatarsals II, III and IV is transversely oval in outline. All proximal articular surfaces exhibit a regular pattern of pits and ridges. The distal articular surface of the metatarsals forms two hemispherical condyles. The transverse diameters of the shafts of metatarsals I to III occupy approximately half of their total length. In metatarsals IV and V, the shaft diameter is approximately one-third of their total length (Figure 8C). The shaft is lateromedially oval in cross-section. In metatarsal I, the shaft is strongly constricted and distally twice as wide as proximally. Metatarsal II is proximally and distally expanded to one-third wider than shaft width, and its shaft is slightly proximodistally twisted. Metatarsal III possesses a straight shaft that is constricted to three-fourths of its proximal and distal width. The proximal end of metatarsal IV is as wide as the shaft, but the distal end is expanded to twice the proximal width. Metatarsal V is small and rod-like, and it is not constricted and bears two weakly rounded distal condyles (Figure 8C).

In anterior and posterior views, the surface of the proximal end of metatarsals II to IV is medially depressed and slightly rough (Figure 8C,D). The distal end of the metatarsals has a roughened distal articular surface.

Pedal phalanges. Pedal digit I possesses two phalanges (Figure 8C). Whereas the proximal phalanx is rod-like and reaches three-fourths of the metatarsal length, the distal phalanx is box-shaped and half as long as it is wide.

Adjacent to metatarsal II lies a box-like proximal phalanx, that bears a distinct lateral and medial condyle (Figure 8C). The distal phalanx is strongly reduced in the pes, sitting distally adjacent to the medial condyle of the proximal phalanx. Metatarsal III possesses a box-shaped proximal phalanx, and at the left tarsus, a distally adjacent ungual phalanx. The ungual phalanx is one-fourth longer than the proximal phalanx, wedge-shaped in distal view and tapers distally only slightly.

Metatarsal IV bears distally an equally long proximal phalanx and a distal ungual phalanx that is half as long as the proximal phalanx (Figure 8C,D). The proximal phalanx is three times as long as it is wide and possesses a shaft that is slightly constricted and ends distally with a lateral and a medial condyle. In the right pes, metatarsal IV bears two scattered remains; a proximal and a distal phalanx.

Histology

As part of a larger sampling programme on sauropod long bone histology, the femur of SMA 0009 was sampled by two of us (MS and NK) using the coring technique developed by Sander (2000). The sample site was in the middle of the shaft, and the core extends from the anterolateral to the posteromedial side of the bone. Due to the small size of the bone (least width at femoral shaft = 34.5 mm), a core diameter of only 4 mm was chosen for this and other similarly small specimens compared to the usual 13 mm diameter cores for large bones. The core was cut lengthwise along the cross sectional plane of the bone and processed into a standard petrographic thin section and a polished section. The sections obtained thus represent a segment of the cross section of the bone at mid-shaft.

The histology of the femur of SMA 0009 was evaluated against core samples from extensive growth series of the humeri and femora of the common sauropods from the Morrison Formation (*Diplodocus*, *Apatosaurus* sp., and *Camarasaurus* sp.; Sander 2000; Sander and Tückmantel 2003), as well as *Brachiosaurus brancai*, *Tornieria Africana*, and *Dicraeosaurus* spp. (Sander 2000). Sander (2000) and Sander and Tückmantel (2003) found a clear correlation between long bone (humerus and femur) histology and body size in all of these taxa. Sander (2000) recognized four ontogenetic stages in sauropod long bone histology, termed 'hatchling' bone, 'juvenile' bone, 'adult' bone, and lamellar-zonal bone. SMA 0009 as well as small sauropod long bones from Kenton area, Oklahoma (*Apatosaurus* humerus OMNH 1278, 258 mm long; *Apatosaurus* femur OMNH 1279, 340 mm long; *Camarasaurus* humerus OMNH 2115, 227 mm long) (see Carpenter and McIntosh 1994) and a humerus from the Dry Mesa Quarry (indet. sauropod, BYU 16929, 180 mm long) all show the same general histology corresponding to the 'hatchling' or 'juvenile' bone of Sander (2000).

The tissue of the bone cortex of the femur SMA 0009 (Figure 9) consists exclusively of fibrolamellar bone that is characterised by a poorly organised arrangement of the vascular system in the innermost cortex as is characteristic of 'hatchling' bone. Most of the cortex thickness of 9 mm shows a laminar arrangement of the vascular system, however. The bone between the vascular canals is exclusively of the fibrous kind, and primary osteons lining the vascular canals had not yet developed. The vascular canals are relatively large, giving the tissue a very high porosity. Osteocytes are represented by their lacunae and were plump and numerous (Figure 9). There are no lines of arrested growth. In the inner cortex, there are large resorption rooms, and the medullary region seems to have been filled by trabecular bone (diagenetically collapsed).

The presence of these tissue types indicates that SMA 0009 represents an early juvenile, but the laminar arrangement of the vascular canals except for the innermost cortex (Figure 9) suggests that it was beyond the hatchling stage. The lack of any lines of arrested growth seems to indicate that the specimen

was less than one year old. However, precise aging is not possible because growth marks such as lines of arrested growth are commonly lacking in the cortex of larger specimens, as well and may not be consistently expressed (Curry 1999; Sander and Tückmantel 2003). The type of tissue observed in SMA 0009 and other small sauropods from the Morrison Formation is consistent with the early juvenile histology of other dinosaurs (Horner et al. 1999, 2000; Padian et al. 2001; Padian et al. 2004). In conclusion, bone histology unequivocally indicates that SMA 0009 is an early juvenile, but a precise ontogenetic age cannot be given at this time.

Discussion

Taxonomy

A taxonomic assignment of SMA 0009 is challenging, because this sauropod individual is an early juvenile and many of its skeletal characters are still likely to undergo ontogenetic changes. Direct comparison of SMA 0009 with other adult sauropod skeletons is therefore difficult. A number of characters indicates that SMA 0009 might belong to Diplodocidae (Table II). However, two distinct features of Diplodocidae and Diplodocinae are not present: 1.) Resulting from short cervical centra, SMA 0009 has a remarkably short neck relative to overall body size in comparison with any known adult diplodocid skeleton from the Morrison Formation. This feature seems to relate to a strong positive allometric growth, but not to an autapomorphy of this taxon (see discussion in 'Ontogeny of early juvenile sauropods'). 2.) Pneumatic fossae or lateral concavities are absent in the anterior caudal vertebrae of SMA 0009. Although the presence of such pneumatic fossae is thought to be diagnostic for Diplodocidae and Diplodocinae (Wilson 2002) (Table II), it should be noted that pneumatic fossae are also absent in the anterior caudal vertebrae of *Apatosaurus* (McIntosh 1990a,b; Upchurch et al. 2004a). SMA 0009 may have shared this absence as a synapomorphy with *Apatosaurus*, or pneumatic fossae might due to its early ontogenetic stage not have been well-developed in SMA 0009 (see discussion in 'Pneumatic structures in the vertebrae' below). However, without information on the anterior caudal vertebrae of early juveniles of either *Barosaurus* or *Diplodocus*, a definite conclusion cannot be reached here.

Comparison with other Morrison diplodocid genera

Here, we compare SMA 0009 with other diplodocid genera, primarily from the Late Jurassic Morrison Formation of North America, such as *Apatosaurus*, *Barosaurus*, and *Diplodocus*. The taxa *Suuwassea*, *Apatosaurus* (*Eobrontosaurus*, Bakker 1998) *yahnahpin* and *Haplocanthosaurus* (although the phylogenetic position of this taxon is far from clear), are also interesting, as they are found in the Lower Morrison Formation like SMA 0009.Overall, SMA 0009 has mosaic characteristics of both *Apatosaurus* and *Barosaurus* that strongly indicate an evolutionary relationship. As this early juvenile skeleton also has a number of significant features separating it from other known Morrison sauropods, we suggest two possible explanations. 1.) SMA 0009 might belong to an unknown taxon or 2.) SMA 0009 shows strong ontogenetic modifications due to its early ontogenetic age. Both possibilities are discussed in the next sections.

Table II. Comparisons of synapomorphies of various diplodocid clades with SMA 0009. Characters are based on Wilhite (1999), Appendix 3).

Subgroups	Character #	Presence or absence in SMA 0009
Diplodocoidea	1	Not present; cervical ribs about 1.8 times as long as centrum
Diplodocidae + Dicraeosauridae	1–9, 14–17	Unknown
	10	Not exposed
	11	Not present; sacral neural spines with about the same length as centra
	12	Present; fairly developed
	13	Present, in Ca-1-Ca-3
	18	Present
Diplodocidae	1–9, 15, 16	Unknown
	10	Present; probably nine dorsal vertebrae
	11	Present
	12	Not present; note that this character is also absent in most *Apatosaurus* specimens
	13	Present
	14	Present (?)
Diplodocinae	1	Not present; relatively short cervical centra
	2	Not present; note that this character is also absent in most *Apatosaurus* specimens
	3	Not present
	4	Uncertain
	5	Not present; laterally and ventrally concave
	6	Present
	7	Present

Cervical vertebrae. SMA 0009 has relatively short mid-cervical vertebrae with an EI of Cep-1 of 1.67, whereas it is 3.0 in the 7th cervical vertebra of *Suuwassea*† (Harris and Dodson 2004; Harris 2006b). In SMA 0009, the EI of Cep-7 is 1.62 (Table III), which is close to an EI value of 1.57 in the 14th cervical vertebra of an adult *Apatosaurus* (NSMT-PV 20375) (Upchurch et al. 2004b) and to the vertebral centra of an early juvenile *Apatosaurus* (OMNH 1246) (Carpenter and McIntosh 1994). The EI is greater than 2.0 in the posterior cervical vertebrae of *Diplodocus* (Hatcher 1901) and *Barosaurus* (Lull 1919; McIntosh 2005).

SMA 0009 has a median keel on the ventral surface of the centra as present in *Barosaurus* (Lull 1919) and *Apatosaurus* (Upchurch et al. 2004b). The simplicity of the pneumatic fossae at the vertebral centra of SMA 0009 contrast the more complex and subdivided pneumatic fossae and foramina at the lateral surface of the cervical vertebral centra of adult Diplodocidae (McIntosh 2005), which is probably an ontogenetic effect.

Cervical ribs. The slender elongate cervical ribs of SMA 0009 are in strong contrast to the short and blunt cervical ribs of *Apatosaurus* (Upchurch et al. 2004b). The long and narrow anterior process of the cervical ribs in SMA 0009 resembles those of the cervical vertebrae of *Diplodocus carnegii* (Hatcher 1901; Holland 1906) and *D. longus* (Marsh 1896; Hatcher 1901), but the long rod-like distal shaft of the cervical ribs of SMA 0009 strongly differs from *Diplodocus* (Gilmore 1936; McIntosh 1990b). In contrast to SMA 0009 *Suuwassea* possesses no extended anterior rib process (Harris and Dodson 2004; Harris 2006b).

The anterior rib process may vary among different positions of a neck (Wedel and Sanders 2002), and this feature may be less reliable for understanding the relationship in diplodocids. Nevertheless, the overall morphology of the rib-shaft is considered here to be beyond ontogenetic variability, making the general morphology and proportions of cervical ribs a useful diagnostic character. It should be noted that the slender cervical ribs found in SMA 0009 are similar to *Camarasaurus* (Gilmore 1925; McIntosh et al. 1996) and *Brachiosaurus* (Janensch 1950), except for a much longer rib-shaft exceeding two centra in length.

Dorsal vertebrae. The estimated total of nine dorsal vertebrae of SMA 0009 is similar to *Barosaurus* (McIntosh 2005). SMA 0009 is different from all other sauropods in possessing very elongate dorsal centra, with an EI ranging from 1.28 to 2.13 (Tables I and III). This unique feature of SMA 0009 most likely represents strong negative allometric growth (see below 'Ontogeny of early juvenile sauropods').

Dorsal ribs. The anterior dorsal ribs of SMA 0009 are morphologically similar to those of *Barosaurus* and *Apatosaurus* (McIntosh 2005), especially in the wide separation of the rib head and tuberculum. SMA 0009 has dorsal ribs with an L-shaped cross-section near the proximal portion of the rib shaft, resembling the anterior dorsal ribs of most diplodocids (Hatcher 1901; Upchurch et al. 2004b; McIntosh 2005: fig 2.7).

SMA 0009 does not possess pneumatic fossae or foramina in the dorsal rib heads, the presence of which is thought to be an autapomorphy for Titanosauriformes (Wilson 2002). It should be noted that pneumatic foramina in dorsal ribs are also known from fully-grown individuals of *Supersaurus* (Jensen 1985; Lovelace et al. 2005) and some individuals of *Apatosaurus* (Marsh 1898; Gilmore 1936; Upchurch et al. 2004b). Thus, it is possible that pneumaticity of the ribs was not as well developed in the early juvenile sauropod SMA 0009 as it was in adult diplodocids.

Sacral vertebrae. The neural spines of the five sacral vertebrae of SMA 0009 are remarkably short (ca. 2/5 of the total height of the vertebra), but anteroposteriorly elongate (ca. 3/4 of the total length of the vertebra). In contrast, tall neural spines are though to be a synapomorphy of the clade Diplodocidae plus Dicraeosauridae (Wilson 2002). *Haplocanthosaurus* (Hatcher 1903) possesses similarly short and long neural spines, which have in contrast to the convex dorsal margin in SMA 0009 a straight dorsal margin. The short neural spines found in SMA 0009 possibly indicate strong positive allometric growth, but may also represent a diagnostic character for this taxon.

Caudal vertebrae. The nearly planar posterior articular surface of the anterior caudal vertebrae of SMA 0009 differs from the convex posterior articular surface in diplodocids and dicraeosaurids (McIntosh 1990b; Upchurch et al 2004a). In SMA 0009, all centra have a smooth flat lateral surface, whereas *Barosaurus*, *Diplodocus*, and *Haplocanthosaurus*, possess a developed horizontal ridge in the anterior to mid-caudal vertebrae (Upchurch et al. 2004b).

The ventral surface of the mid-caudal vertebrae is longitudinally concave in SMA 0009, but not much weaker than *Diplodocus* and *Barosaurus* (McIntosh 2005). Similar relatively shallow longitudinal depressions are also known from *Apatosaurus*. The isolated mid-caudal vertebrae of SMA 0009 have a relatively short centrum, which is more similar to *Apatosaurus* than to *Diplodocus* and *Barosaurus*.

The anterior caudal vertebrae of SMA 0009 possess wing-like transverse processes, as commonly found in Dicraeosauridae and Diplodocidae (Wilson 2002). In SMA 0009, such wing-like transverse processes are restricted to the anteriormost three caudal vertebrae,

Table III. Comparisons of juvenile diplodocid (SMA 0009) with other diplodocids from the Morrison Formation.

Characters	**SMA 0009**	***Apatosaurus***	***Barosaurus***	***Diplodocus***	***Suuwassea***
EI in posterior cervical vertebra	1.6	1.57	1.9	2.0	3.0
Prezygapophyses exceed anterior vertebral centrum in cervical vertebrae	Yes	No	No	Yes	Yes
Ratio of cervical rib to centrum length	>1.6	<.8	Not known	<1.0	<1.0
Anterior rib process in cervical ribs	Long	Variable	Long	Variable	Short
EI in posterior dorsal vertebra	1.5	.8	.9*	.9	?
Pneumatic foramina in dorsal ribs	No	Yes	No	No	No
Ratio of neural spine to vertebral height in sacral and anteriror caudal vertebrae	<.4	>.4	>.4	>.4	?
Centrum of anterior caudal vertebrae Amphicoelous	Weakly amphicoelous	Weakly procoelous	Procoelous	?	
Horizontal ridge on lateral surface of anterior to mid-caudal vertebrae	Absent	Present	Present	Present	Present
Occurrence of transverse processes in anterior caudal vertebrae	Ca1-Ca7	Ca1-Ca12/14	Ca1-Ca15/18	Ca1-Ca15/18	?
Overall shape of coracoid	Circular	Rectangular	Circular	Circular	Rectangular
Glenoid surface of scapula and coracoid sharing similar in length	Yes	No	No	No	Yes
Limb bones	Gracile	Robust	Gracile	Gracile	Robust
Ratio of deltopectoral crest length to total humerus length	.3	.45	.45	.4	ca. .35
Pubic peduncle of ilium	Elongate	Short	Short	Short	Short
Medial process on astragalus	Long, slender	Long, slender	Long, slender	Short, massive	?
Bridge from metatarsal I to II	Well developed	Poorly developed	Poorly developed	Well developed	Well developed

*EI is similar to anterior dorsal vertebrae.

similarly to *Apatosaurus* (McIntosh 1981; Upchurch et al. 2004b). However, the caudal vertebrae of SMA 0009 bear transverse processes only between Ca-1 and Ca-7, whereas in *Apatosaurus* the anterior 12 to 14 caudal vertebrae bear transverse processes (Upchurch et al. 2004b), in the basal neosauropod *Haplocanthosaurus* the anterior 12 (Hatcher 1903), and in *Diplodocus*, *Barosaurus* and *Dicraeosaurus* even the anterior 15 to 18 caudal vertebrae (Table III).

No other diplodocid specimens have such anteroposteriorly long but short neural spines in the tail base like in SMA 0009 (Table III). These neural spines resemble in height those of *Haplocanthosaurus* and *Camarasaurus*. Either the height of the neural spines dramatically increases during the ontogeny of diplodocids including SMA 0009, or short neural spines in SMA 0009 are a diagnostic character for this taxon, explained as peramorphosis related to heterochrony (Salgado 1999).

The mid-caudal neural spines of SMA 0009 exhibit a straight posterior margin and a slight caudal inclination, resembling those of *Apatosaurus* and *Diplodocus* (Upchurch et al. 2004b). In *Barosaurus*, the posterior margin of the mid-caudal neural spines is slightly more convex, and the mid-caudal vertebrae of *Seismosaurus* are considerably taller (Gillette 1991). In comparison with SMA 0009, the mid-caudal neural spines are more posteriorly inclined and longer in *Dicraeosaurus*.

Terminally to Ca-7, the lateral surface of the neural spines in SMA 0009 bears no spinoprezygapophyseal laminae, whereas the last appearance of this lamina is Ca-8 in *Apatosaurus excelsus* (CM 563; Gilmore 1936), Ca-14 in *Diplodocus longus* (AMNH 223; Osborn 1899), and Ca-13 in *D. carnegii* (CM 94; Hatcher 1901). This might indicate a close connection between the development of vertebral laminae and ongoing pneumatisation of the sauropod skeleton during growth (see 'Pneumatic structures in the vertebrae' below).

Scapula and coracoid. The scapula of SMA 0009 is 28% longer than the femur. Such a relatively large scapula is unique for sauropods. The overall scapular morphology is very similar to other diplodocids, such as a juvenile (CM 566)[‡] and adult (CM 564, 3018) *Apatosaurus* and *Suuwassea* (ANS21122). The anterior tuberosity on the mildly expanded distal scapular blade found in SMA 0009 is similarly present in *Apatosaurus ajax* (NSMT-PV 20375; Upchurch et al. 2004b). The angle between acromion ridge and scapular shaft in SMA 0009 is about 90°, resembling juvenile *Apatosaurus* (CM 566, CM 563; Upchurch et al. 2004b) and MWC 1848 (Foster 2005), but being less acute in *Diplodocus* (about 80°; CM 94), *Barosaurus* (about 70°; AMNH 6341), *Suuwassea* (about 80°; ANS21122) and adult *Apatosaurus* spp. (approximately 70°; Upchurch et al. 2004b). The angle of the anterodorsally projecting acromion process of SMA 0009 resembles *Suuwassea* (Harris and Dodson 2004), but this angle varies among six scapulae of *Camarasaurus supremus* (AMNH 5760 and 5761 including three or four individuals) ranging from 80° to 110° (Ikejiri 2004a). Such a large degree of individual variation may infer that this character does not represent a diagnostic feature in the diplodocid genera mentioned above.

SMA 0009 has a subrectangular outline of the coracoid, which is similar to that of *Diplodocus* and *Barosaurus* (Table III), but contrasts the rectangular coracoid of *Apatosaurus* (Upchurch et al. 2004b). The coracoid is approximately as long as the scapular acromion, like in other Diplodocidae, whereas in *Suuwassea* (Harris and Dodson 2004) the anteroposterior length of the coracoid is 24% of the overall scapular length.

The scapulocoracoidal glenoid notch of SMA 0009 is rounded and v-shaped, with the glenoid articular surface of scapula and glenoid having approximately the same length. This is different to other Morrison diplodocids and *Dicraeosaurus*, where the coracoid glenoid surface is half as long as that of the scapula (Upchurch et al. 2004b; McIntosh 2005). Similar long scapular and coracoidal glenoid articular surfaces are present in *Suuwassea* (Harris and Dodson 2004) and *Haplocanthosaurus* (Hatcher 1903).

Forelimb. SMA 0009 has a slender overall shape of the appendicular bones, which are similar to *Diplodocus* and *Barosaurus*, but different to the massive appendicular bones of *Apatosaurus*, *Dicraeosaurus* and *Suuwassea*.

The ratio of 0.8 of the greatest length of the humerus to femur in SMA 0009 is close to *Barosaurus* (Table I; McIntosh 1990b), but considerably differs from *Apatosaurus* (McIntosh 1990b) (Table IV). Although the overall length of the humerus is very close between SMA 0009 and a juvenile *Apatosaurus* (CM 566), the former specimen has a much more slender humerus. The laterodorsal corner of the humeral head in SMA 0009 forms a short projection, which is less expanded than that of *Apatosaurus* and *Suuwassea*. The length of the deltopectoral crest in SMA 0009 is about 30% of the total length of the humerus. This ratio is much smaller (about 45%) in *Barosaurus* (McIntosh 2005) and *Apatosaurus* (Gilmore 1936; Upchurch et al. 2004b) including the early juvenile CM 566 (Table III).

The possession of only one carpal bone in SMA 0009 is similar to *Apatosaurus*, *Barosaurus* (McIntosh 2005) and *Diplodocus* (Bedell and Trexler 2005). The metacarpals of SMA 0009 are slender and elongate, as in *Barosaurus* (McIntosh 2005), but unlike the heavily-built metacarpals in *Apatosaurus*. The ratio

Table IV. Comparison of greatest lengths of appendicular bones in the juvenile diplodocid SMA 0009 and other diplodocids.

Taxon	hu:fe	mc-II:ra	ul:hu	scap:il	scap:fe	ti:fe	mt-II:ti
SMA 0009	.81	.33	.75	1.90	1.38	.83	.22
*Apatosaurus**	.65	.37	?	?	?	.63	?
Apatosaurus excelsus (Yates and Vasconcelos 2005z)**	.62	?	.76	1.26	.89	.72	?
Apatosaurus excelsus (CM 566)***	.67	?	?	?	.96	?	?
Apatosaurus louisae (CM 3018)**	.64	.34	.74	1.11	.92	.62	.20
*Diplodocus**	.65	.30	?	?	?	.69	?
Diplodocus longus (AMNH 5855)**	.62	?	.82	?	?	.69	?
Diplodocus carnegii (CM 94)**	?	?	?	1.28	1.11	.67	.17
*Barosaurus**	.71	?	?	?	?	.73	?
Barosaurus lentus (AMNH 6341)**	.75	?	?	?	1.19	.75	?

Data from *McIntosh (1990a), **Bonnan (2001), and ***Peterson and Gilmore (1902).

of the greatest length of metacarpal II and radius in SMA 0009 resembles *Apatosaurus* (CM 3018) and *Diplodocus* (Table IV) (McIntosh 1990b: Table 4.1).

Ilium. The elongate iliac body and extremely elongate pubic peduncle of SMA 0009 resembles brachiosaurid dinosaurs, such as *Brachiosaurus altithorax* (Riggs 1903; Jensen 1987), an indeterminate brachiosaurid (Jensen 1987), and a juvenile brachiosaurid (BMNH R12713; Blows 1995). In the Morrison diplodocids, *Barosaurus* (AMNH 6341) tends to have a relatively elongate pubic peduncle (AMNH 6341; McIntosh 1990a, 2005). The pubic peduncle of adult and juvenile *Apatosaurus* (Carpenter and McIntosh 1994) is one-fourth shorter than in SMA 0009 relative to the overall length. An elongate pubic peduncle as in SMA 0009 seems to be unique, and may not relate to strong allometric growth because no juvenile diplodocid is known to have this feature. The ilium of SMA 0009 contrasts *Barosaurus* in its more indented posterior iliac part and a pointed posterior process being more similar to *Apatosaurus*.

Hind limb. The femur of SMA 0009 has a slender shaft, similar to *Barosaurus* (e.g., AMNH 6341, McIntosh 2005) and *Diplodocus*. Although SMA 0009 shares a similar humeral length with the juvenile *Apatosaurus* CM 566 (Table VI), the femora of both taxa considerably differ in length. CM 566 has a considerably longer femur than SMA 0009.Also, the mid-shaft of the femur of SMA 0009 is very slender, which is similar to *Barosaurus* or *Diplodocus*, but contrasts the massive or robust, heavily-built femora in *Apatosaurus* including CM 566.SMA 0009 also differs from the 'stove-pipe' type-femur of *Amphicoelias*, characterized by a nearly circular cross section of the mid-shaft (McIntosh 2005).

The ratio of the tibia to femur is with 0.83 in SMA 0009 the highest among the Morrison diplodocoids (Table IV). *Barosaurus* (AMNH 6341; McIntosh 1990b) has the closest ratio (0.75) to SMA 0009 (Table IV). As a typical diplodocid character, the fibula of SMA 0009 has a straight shaft (Wilhite 2005) that tapers continuously from proximally to distally. This is in contrast to the deflected fibular shaft of *Haplocanthosaurus* (Ikejiri, personal observation) and *Camarasaurus* (Ikejiri et al. 2005b: fig. 6.10.G).

The astragalus of SMA 0009 has a longer and more slender medial process than *Diplodocus*, being more similar to that of *Apatosaurus* and *Barosaurus* (McIntosh 2005). In contrast, in *Apatosaurus*, the medial cotyle bears no foramina (Wilson 2002; Bonnan 2003). The astragalus of SMA 0009 is similar to that of *Barosaurus* in its slender and projecting medial process, a rounded distal roller, and a perforated medial fossa on the tibial articular surface.

The distal process from metatarsal-I that forms the metatarsal 'bridge' to metatarsal II is as strongly developed in SMA 0009 as in *Barosaurus* (AMNH 6341, CM 11984) and *Suuwassea* (ANS 21122; Harris and Dodson 2004), whereas this process is weaker in *Apatosaurus* and *Diplodocus*. Furthermore, metatarsal-I is relatively more elongate in SMA 0009 and not as stout as in *Apatosaurus*.

Unique features in SMA 0009

The following features of SMA 0009 differ from any other known diplodocid from the Morrison Formation: (1) relatively short neck, (2) elongate cervical ribs (1.5 to 2 times the length of the centrum), (3) elongate centra in the mid- and posterior dorsal vertebrae (EI ranging from 1.28 to 2.13), (4) relatively short neural spines in the sacral and anterior caudal vertebrae, (5) very large scapula, (6) small coracoid with semi-circular outline, and (7) relatively elongate lower hind limb (fibula-to-femur ratio = 0.78). These unique features may indicate that SMA 0009 is an unknown diplodocid genus. However, if these characters are all preserved in such an ontogenetically young specimen, how can identification and definition of this taxon be reliably based on comparisons of with other diplodocids consisting of mostly adult individuals? Without a better understanding of early juvenile ontogenetic variation, taxonomic assignment of SMA 0009 is very difficult.

Ontogeny of early juvenile sauropods

Beside a number of isolated bones, skeletons of early juvenile sauropods (i.e., approximately lower than 100 cm in shoulder height or younger than a few years olds) are very rare, limiting information on early juvenile sauropods. Only partial skeletons have been reported, such as an indeterminate sauropod from the Upper Cretaceous of India (Mohabey 1987), *Alamosaurus* from the Upper Cretaceous of Texas (Lehman and Coulson 2002), and *Apatosaurus* sp. from the Late Jurassic of Wyoming (Peterson and Gilmore 1902). Furthermore, as taxonomic assignment of SMA 0009 is uncertain, comparisons of this juvenile specimens with adult individuals is difficult.

Two different ideas for determination of significant ontogenetic signals appearing in SMA 0009 are used. First, ontogenetic variation found in other Morrison diplodocid taxa (especially *Apatosaurus* and *Barosaurus*) is compared to SMA 0009. Particularly, an early juvenile (CM566) and fully grown (CM 563) *Apatosaurus* sp. from a single quarry are important, because this juvenile *Apatosaurus* is about the same body size as SMA 0009, and SMA 0009 is thought to be closely related to *Apatosaurus*. Second, ontogenetic changes appearing in juvenile to adult *Camarasaurus* are compared with SMA 0009 to examine whether or not similar patterns of ontogenetic changes occurred in *Camarasaurus* and SMA 0009. *Camarasaurus*, including the three most common species *C. grandis*, *C. lentus*, and *C. supremus*, consists of one of the largest sample sizes of various ontogenetic series in sauropods (Ikejiri et al. 2005b). Some important ontogenetic modifications are found, such as (1) degree of neurocentral fusion, (2) closure of foramina, (3) texture of articular surfaces of bones, and (4) relative growth of bones (Ikejiri 2003, 2004a,b).

Degree of postcranial skeletal fusion. The degree of fusion between centrum and neural arches in the presacral to anterior caudal vertebrae, and between scapula and coracoid are useful to identify relative maturity in sauropods, such as *Alamosaurus*, *Apatosaurus*, *Brachiosaurus*, and *Camarasaurus* (Ikejiri, personal observation). Based on the condition of the postcranial skeletal fusion in these sauropods, SMA 0009 shows typical immature characters, as especially in the presacral vertebrae the neural arches and centra are unfused or display a visible neurocentral suture.

Ikejiri (2003) established as three stages of skeletal fusion in reptiles unfused (1st: physically separated elements), closed (2nd: visible neurocentral suture present), and fused vertebral elements (3rd: completely fused elements with no suture). Unfused vertebral elements are though to be an intermediate condition during a life. In SMA 0009, the neurocentral suture is visible from Ca-1 to Ca-10, and more posterior caudal vertebrae display complete fusion between neural arch and centrum (Figure 6G–J). Since caudocervical fusion is known in the caudal vertebrae of the sauropod *Camarasaurus* (Ikejiri et al. 2005b), as well as in most other reptiles (such as extant crocodylians (Ikejiri, personal observation) and hadrosaurs (Horner and Currie 1994)), the same sequence seems to occur in the caudal vertebrae of SMA 0009.However, no articulated caudal vertebrae are known in juvenile diplodocids from the Morrison Formation. In the juvenile *Camarasaurus lentus* (CM 11338), the anterior six to seven caudal vertebrae have a visible neurocentral suture.

In SMA 0009, the cervical vertebrae have unfused centra and neural arches (Figure 5E), but the dorsal vertebrae seem to have a closed (patent) neurocentral suture. Identification of vertebral fusion is slightly difficult in the dorsal vertebrae of SMA 0009 because of their articulation. Additionally, matrix may fill the space between the neural arch and centrum, which would attach the elements tightly to each other. However, cervicocaudal fusion is reported in *Camarasaurus* (Ikejiri et al. 2005b), and this may be also true in SMA 0009.

The left scapula and left coracoid are unfused in SMA 0009, which is typically found in immature sauropods. Fusion between scapula and coracoid is only found in mature individuals of *Camarasaurus*, and is thought to be one of the key characters to separate subadults and adults (Ikejiri 2004a: 'stage 2').

Closure of coracoid foramen. An open coracoid foramen at the edge of the scapular articular surface is found in a juvenile *C. lentus* (CM 11338), and might be a typical juvenile feature in sauropods (Ikejiri 2003; 2004a). In fact, the left coracoid of SMA 0009 has only a shallow, grove-like concavity extending transversely along the scapula articular surface (Figure 4B,C). Although the right isolated coracoid has a closed coracoid foramen, this feature seems to be questionable as an indicator of ontogenetic stages. The coracoid is apparently deformed during processes of fossilization and the entire bone surface is weathered, making examination of this feature difficult.

Texture of articular surface of limb bones. Comparisons of proximal ends of the femora of juvenile, subadult, and fully grown individuals of *Camarasaurus* showed that articular rugosities of mature specimens exhibit many well-developed pits and grooves (Ikejiri 2004a). Similar developmental patterns of limb articular surfaces are known from various juvenile extant birds (Geist and Jones 1996). Apparently, SMA 0009 possesses relatively smooth limb articular

Figure 10. Comparison of articular surfaces of limb bones of juvenile to adult sauropods. Proximal end of the femur of (A) early juvenile diplodocid SMA 0009; (B) juvenile *Camarasaurus lentus* (CM 11338); (C) fully-grown *C. lentus* (WDC A: BS-157). Scale bar is 5 cm. B and C from Ikejiri (2004a).

surfaces (Figure 10), comparable to juvenile *Camarasaurus* and *Phuwiangosaurus sirindhornae* from Thailand (Martin 1994).

The relatively flat proximal end of metacarpal I does not possess a developed medial ridge (Figure 9C,D), which is commonly found in mature sauropods. A number of small pits, typical for the carpals of adult sauropods, are also under-developed in SMA 0009.

Relative growth. One of the most striking features found in SMA 0009 are its body proportions, such as the short neck. A mature dicraeosaurid, *Brachytrachelopan*, from Argentina is known to have a particularly short neck among sauropods (Rauhut et al. 2005), but this sauropod taxon has not been reported from North America. In contrast to the short cervical vertebrae, SMA 0009 has extremely elongate mid- and posterior dorsal centra, which contrast any known adult diplodocids. Among juvenile and adult *Camarasaurus*, strong positive allometric growth is found in the axis and mid-cervical vertebrae, referring to a relative elongation of the neck, but negative allometry in the anterior dorsal vertebrae, referring to a relative shortening of the trunk (Ikejiri 2004a,b). Based on the information above, we suggest that the unique vertebral proportions found in SMA 0009 might have occurred in various groups of sauropods during an early juvenile stage.

The remarkably elongate cervical ribs of SMA 0009, compared to adult diplodocoids from the Morrison Formation, may indicate strong negative allometric growth during the early juvenile stage. In *Camarasaurus lentus*, a late juvenile specimen (CM 11338) already has elongate cervical ribs as found in other adult individuals (Ikejiri 2004a,b). However, well-preserved nearly complete cervical ribs are rarely found in juvenile sauropods, so that it is uncertain whether or not this feature is universal across a wide range of sauropod taxa.

A relatively large elongate scapula as found in SMA 0009 seems to be a typical early juvenile sauropod feature. Negative allometric growth is thought to occur during the ontogeny of *Camarasaurus* (Ikejiri 2004a,b), and a relatively elongate scapular blade is also reported in another early juvenile sauropod (Mohabey 1987).

As discussed above, SMA 0009 has unique proportions in the limb bones among the Morrison diplodocids. Although articulated limb elements are rare in early juvenile diplodocids, it should be addressed that the juvenile *Apatosaurus* CM 566 (225 mm in humeral length, which is only 20% longer than SMA 0009), shares similar proportions among the humerus, ulna, radius, and femur with the adult specimen CM 563. Based on this single evidence, we suggest that isometric growth occurs in these limb bones of early juvenile to adult diplodocids. The ratio of the forelimb bones to femur therefore seems to be a useful parameter for identifying early juvenile diplodocids at the generic level, and SMA 0009 possibly represents an unknown diplodocid taxon.

Pneumatic structures in the vertebrae

The divided pneumatic fossae with pneumatic foramina at the cervical vertebrae, the presence of distinct pneumatic fossae in Do-1 to Do-4, and the laminae in all presacral vertebrae are indications for the presence of vertebral pneumaticity in the skeleton

of SMA 0009. In an early juvenile sauropod with not fully pneumatised vertebrae, those vertebrae having the longest contact to the pneumatising epithelium would be more excessively pneumatised than other bones. Thus, the maximum of pneumatic structures in the posteriormost cervical vertebrae of SMA 0009 most plausibly indicates the starting point for vertebral pneumatisation from a paired cervical air sac in the shoulder region, as in extant birds (Müller 1908; Cover 1953; Hogg 1984; O'Connor 2003, 2006) and other sauropods (Wedel 2003a,b). The presence of pneumatised dorsal vertebrae in this early juvenile sauropod supports the idea that sauropod lungs, which must have been located in the anterior trunk portion, had contact to the dorsal vertebral column (Perry and Reuter 1999; Wedel 2003b; Perry and Sander 2004).

The presence of pneumatic foramina and deep pneumatic fossae on the cervical vertebral centra makes it plausible that pneumatic diverticula had already started to expand laterally along the cervical vertebral column of SMA 0009. In contrast, the diapophyses and neural arches of the cervical vertebrae show no unequivocal osteological features indicating intraosseous pneumatisation (O'Connor 2003, 2006). It can be assumed that the neural arch region with the diapophyses was pneumatised after the vertebral centra.

The presence of large pneumatic fossae occupying most of the lateral surface of the vertebral centra in the cervical vertebrae of SMA 0009 is consistent with the distribution of pneumatic fossae found in the cervical vertebrae of early juvenile *Apatosaurus* and *Camarasaurus* (Wedel et al. 2000b). The pneumatisation pattern of the cervical vertebrae of early and late juvenile diplodocids is much simpler than in the cervical vertebrae of adults (Figure 6E; Wedel 2003a; Schwarz et al. 2004). Thus, comparing cervical vertebrae of early juvenile (e.g., SMA 0009; Carpenter and McIntosh 1994; Ikejiri 2004a,b), subadult (Wedel 2003a; Schwarz et al. 2004) and adult (Wedel et al. 2000b; Wedel 2003a; Schwarz et al. 2004) sauropods with a camerate internal pneumatisation pattern, there seems to be a tendency in initial pneumatisation to form large and simple pneumatic fossae and camerae until a first equilibrium is reached in the relationship between bone and pneumatic space.

Only a weak lamination of the neural arches as well as a slight depression at the lateral surface of the vertebral centra is present in the sacral and anterior caudal vertebrae. This might indicate starting pneumatisation. Vertebral laminae are present even in the most basal sauropods, probably as partitioning structures between pneumatic diverticula (Wilson and Sereno 1998; Wilson 1999; Wedel 2003a). The absence of pneumatic fossae and distinct lamination of the neural arch in the caudal vertebrae of SMA 0009 could indicate that pneumatic diverticula have just entered the sacrocaudal region and did not resolve much bone material. This hypothesis would lead to the conclusion that pneumatic diverticula in the anterior caudal vertebrae extended very quickly from ventrally to dorsally, so that the lamination of the neural arch would have proceeded simultaneously to the formation of pneumatic fossae at the vertebral centrum. It would mean that even before developing pneumatic fossae, pneumatic diverticula would have spread dorsally to the neural arch. This would be a contradictory development to the cervical vertebrae, where the vertebral centrum is pneumatised prior to the neural arch.

A more likely hypothesis for the presence of vertebral laminae in the sacral and anterior caudal vertebrae is that lamination is already detectable even in non-pneumatised vertebrae. In this case, laminae would not be formed exclusively by pneumatic diverticula, but be present before, probably even at a hatchling stage. Laminae would then provide a kind of 'pathway' for the growing pneumatic diverticula (Wilson 1999). This would be consistent with the hypothesized functions of the vertebral laminae as structural elements for stress-resistance in the vertebrae and as osseous septa of the pneumatic cavities (Witmer 1997; Wilson 1999; Wedel 2003a). It would also explain the determined position of the laminae in the vertebrae of sauropod taxa making their landmark-based definition (Wilson 1999) and taxonomic value (Wilson 1999, 2002) possible. Since development of vertebral laminae is linked with vertebral pneumaticity (see below) (Wilson 1999; Wedel 2003a), in such early juvenile specimens not all of these laminae might be present. This could mean that in these individuals only the presence of laminae would be diagnostic, whereas their lack would not. However, this hypothesis could only be tested at a growth-series of sauropod skeletons of the same taxon, which are recently not available.

As a third hypothesis, the lack of pneumatic fossae at the vertebral centra of the anterior caudal vertebrae could be taxonomically significant for SMA 0009. In fact, among diplodocids, *Seismosaurus* and *Apatosaurus* have anterior caudal vertebrae lacking pneumatic fossae on the lateral surface of the vertebral centra (Gillette 1991; Upchurch et al. 2004b). However, because the pneumatisation process in SMA 0009 was obviously in an early ontogenetic stage, the reliability of this hypothesis cannot be proved.

The absence of vertebral pneumaticity in the sacral and caudal region of the early juvenile sauropod SMA 0009 is difficult to interpret. In contrast to theropods, which exhibit clear osteological correlation for the presence of abdominal air sacs (O'Connor and Claessens 2005), such abdominal air sacs in sauropods could not be reconstructed from strong osteological and ontogenetic evidence (Wedel

2003b). Pneumatisation of the presacral and sacral vertebral column in sauropods could have been brought about by cervical air sacs exclusively (Wedel 2003b), which would speak together with the lacking osteological evidence against the presence of abdominal air sacs in SMA 0009. Alternatively, the assumption of bird-like air sacs in sauropods would make the presence of abdominal air sacs at least possible. SMA 0009 indicates that pneumatisation of the vertebral column in the sacral and caudal region at least in diplodocids might have developed significantly later than in the presacral vertebrae, similar to extant birds (Wedel 2003a). Although we have to wait to test this hypothesis until examining adult specimens of this taxon or reliable taxonomic identification of SMA 0009, the juvenile specimen here sheds a light to the early ontogeny of sauropod pneumaticity.

Conclusions

The complete postcranial skeleton of the early juvenile sauropod SMA 0009 gives significant information for understanding the early ontogeny and taxonomy of diplodocids. SMA 0009 has typical juvenile sauropod features; for example, a visible neurocentral suture in all the presacral, sacral, and anterior caudal vertebrae, smooth articular surfaces of the long limb bones, and unfused scapula and coracoid. Growth patterns of the femur indicates that SMA 0009 is an early juvenile, at least younger than a few years.

The specimen exhibits a number of diplodocid features, such as the elongate slender scapular blade, nine dorsal vertebrae, and the presence of the posterior centroparapophyseal lamina in the posterior dorsal vertebrae. Because SMA 0009 has considerably elongate cervical ribs relative to the centrum length, either the character of short cervical ribs, thought to be the only synapomorphy in Diplodocoidea, may need to be re-considered, or these long cervical ribs are a factor of strong negative allometric growth.

Three diplodocid genera, *Apatosaurus*, *Barosaurus*, and *Diplodocus* are known from several fossil sites near the Howe Ranch of the Jurassic Morrison Formation. Nevertheless, identification of SMA 0009 even at the generic level is difficult due to large degree of ontogenetic changes during an early juvenile stage. A number of osteological features indicate that SMA 0009 is closely related to *Apatosaurus* and *Barosaurus* (Table III). The features of (1) a large scapula, (2) elongate dorsal vertebrae, and (3) a short neck, tend largely to appear also in other juvenile sauropods, particularly *Apatosaurus* and *Camarasaurus*. However, besides the elongate cervical ribs, this early juvenile specimen exhibits unique features among these Morrison diplodocids. (1) A *Brachiosaurus*-like elongate pubic peduncle of the ilium, (2) relatively elongate forelimb or short hind limb bones (humerus-to-femur ratio 0.87), and (3) short neural spines in the sacral and anterior caudal vertebrae cannot be explained by information based on other juvenile sauropods, indicating that SMA 0009 may be an unknown diplodocid genus. It should be noted that several skeletons of mature diplodocids were also collected from the Howe Ranch. Until we fully study the Howe Ranch specimens that may include the same taxon as SMA 0009, we do not make taxonomic assignment of this early juvenile specimen.

Proceeding pneumatisation processes might be responsible for considerable morphological change of the vertebrae (e.g., appearance of certain vertebral laminae). It is possible that early ontogenetic stages of sauropods with a camerate pneumatisation pattern (Wedel et al. 2000a) undergo a similar development of initial pneumatisation, and show a tendency in initial pneumatisation to form large and simple pneumatic fossae and camerae until a first equilibrium is reached in the bone-pneumatic space-relationship. Early juvenile sauropods possessed vertebrae with possibly at least their main laminae forming a kind of 'pathway' for the growing pneumatic diverticula. Lamination of vertebrae in early juvenile sauropod specimens might address taxonomically important features only if present, whereas their absence is possibly less useful for taxonomic assignment.

Acknowledgements

We cordially thank Hans-Jakob 'Kirby' Siber for giving us this great opportunity to study the specimen SMA 0009 and further material at the Sauriermuseum Aathal. Urs Moeckli also supported our visits to SMA. We thank Kenneth Carpenter, John McIntosh, Virginia Tidwell, and Jeffrey Wilson for valuable discussions. Jacques Ayer shared unpublished data on the geology of the Howe Stephens Quarry with us. Peter Larson allowed us to access to the SMA 0009 during a preparation at the Black Hills Institute. For their interest and helpful discussions on the matter we are indebted to David Lovelace, Ray Wilhite, Oliver Wings and the members of the German DFG Research Group (DFG No. 533) 'Biology of the Sauropod Dinosaurs: The Evolution of Gigantism'. Jeffrey Wilson critically reviewed an earlier draft of this manuscript and we wish to thank him for his helpful comments and suggestions for improvement. We also wish to acknowledge the editor Gareth Dyke for his efforts. We thank furthermore the following persons for access to collections under their care: Bernd Herkner (Senckenbergmuseum Frankfurt a.M.), Wolf-Dieter Heinrich, David Unwin (Museum für Naturkunde der HU Berlin), Daniel Brinkman, Walter Joyce (Yale Peabody Museum), Carl Mehling, Mark Norell, Ivy Rutzky (American Museum of Natural History), David Berman, Amy Henrici, Matt Lamanna, Norm Wuerthele (Carnegie Museum of Natural History), Robert Prudy, Michael Brett-Surman (Smithsonian

Institution, Washington DC), José F. Bonaparte, Alejandro Kramarz (Museo Argentino de Ciencias Naturales, Buenos Aires), and Logan Ivy (Denver Museum of Natural History). For this study, DS was financed by the Swiss National Science Foundation (SNF No. 200021-101494/1 and 200020-109131/1). The Wyoming Dinosaur Center research grant partially supported TI.

Notes

†*Suuwassea* was decribed (Harris and Dodson 2004) as belonging to Flagellicaudata with no closer assignment to Diplodocidae or Dicraeosauridae possible. According to a description of the new dicraeosaurid taxon *Brachtrachelopan*, the latest phylogenetic framework on sauropods (Rauhut et al. 2005) and more detailed descriptions of *Suuwassea* by Harris (2006b, 2006a), the taxon might also belong to Diplodocidae, being closely related to *Apatosaurus*.

‡The remains of CM 566 consists of a neural arch of a mid-(?) dorsal vertebra and a number of appendicular bones. This juvenile sauropod was first described as '*Elosaurus parvus*' (Peterson and Gilmore 1902), but revised to be synonymous to *Apatosaurus excelsus* (McIntosh 1981). In a revision of *Apatosaurus*, Upchurch et al. (2004b) again replaced CM 566 and additional material into the new combination *Apatosaurus parvus*, owing to some synapomorphies of the postcranial skeleton. Because the taxonomic assigment of CM566 is still under controversial view, we refer to the remains just as *Apatosaurus* with no species assignment.

References

Ayer J. 2000. The Howe Ranch dinosaurs. Aathal, Switzerland: Sauriermuseum Aathal.

Bakker RT. 1998. Dinosaur mid-life crisis: The Jurassic-Cretaceous transition in Wyoming and Colorado. In: Lucas SG, Kirkland JI, Estep JW, editors. Lower and middle Cretaceous terrestrial ecosystems. Albuquerque: New Mexico Museum of Natural History and Science, Bulletin 14. p 67–78.

Bedell MWJ, Trexler DL. 2005. First articulated manus of *Diplodocus carnegii*. In: Tidwell V, Carpenter K, editors. Thunder-Lizards. The sauropodomorph dinosaurs. Bloomington: Indiana University Press. p 302–320.

Behrensmeyer AK. 1978. Taphonomic and ecologic information from bone weathering. Paleobiology 4:150–162.

Bird RT. 1985. Bones for Barnum Brown: Adventures of a dinosaur hunter. Fort Worth: Texas Christian University Press.

Blows WT. 1995. The early Cretaceous brachiosaurid dinosaurs *Ornithopsis* and *Eucamerotus* from the Isle of Wight, England. Palaeontology 38:187–197.

Bonnan MF. 2001. The evolution and functional morphology of sauropod dinosaur locomotion, PhD thesis, Northern Illinois University.

Bonnan MF. 2003. The evolution of manus shape in sauropod dinosaurs: Implications for functional morphology, forelimb orientation, and phylogeny. J Vert Paleontol 23:595–613.

Bonnan MF. 2004. Morphometric analysis of humerus and femur shape in Morrison sauropods: Implications for functional morphology and paleobiology. Paleobiology 30:444–470.

Breithaupt BH. 1997. Howe quarry. In: Currie PJ, Padian K, editors. Encyclopedia of dinosaurs. San Diego: Academic Press. p 355–356.

Breithaupt BH. 1998. Railroads, blizzards, and dinosaurs: A history of collecting in the Morrison Formation of Wyoming during the nineteenth century. Modern Geol 23:441–463.

Breithaupt BH. 2001. The case of "Big Al" the *Allosaurus*: A study in paleodetective partnerships. In: Santucci VL, McClelland L, editors. Proceedings of the 6th Fossil Resources Conference (National Park Service, U.S. Department of the Interior, Geologic Resources Division Technical Report), p 95–106.

Brown B. 1935. Sinclair dinosaur expedition, 1934. Natural Hist 36:3–13.

Carpenter K, McIntosh JS. 1994. Upper Jurassic sauropod babies from the Morrison Formation. In: Carpenter K, Hirsch KF, Horner JR, editors. Dinosaur eggs and babies. Cambridge: Cambridge University Press. p 265–278.

Chure DJ, Carpenter K, Litwin R, Hasiotis S, Evanoff E. 1998. Appendix. The fauna and flora of the Morrison Formation. Modern Geol 23:507–537.

Claessens LPAM. 2004. Dinosaur gastralia; origin, morphology, and function. J Vert Paleontol 24:89–106.

Colbert EH. 1968. Men and dinosaurs. New York: E.P. Dutton and Co., Inc.

Cover MS. 1953. Gross and microscopic anatomy of the respiratory system of the turkey. III. The air sacs. Am J Vet Res 14:239–245.

Curry KA. 1999. Ontogenetic histology of *Apatosaurus* (Dinosauria: Sauropoda): New insights on growth rates and longevity. J Vert Paleontol 19:654–665.

Curry Rogers KA. 2000. Growth rates among dinosaurs. In: Paul GS, editor. The scientific American book of dinosaurs. New York: St. Martin's Press. p 297–309.

Curtice BD, Foster JR, Wilhite DR. 1996. A statistical analysis of sauropod limb elements. J Vert Paleontol 17:41A.

Dong Z, Zhou S, Zhang Y. 1983. The dinosaurian remains from Sichuan Bain, China. Palaeontol Sinica C 23:139–145.

Erickson GM, Curry Rogers KA, Yerby SA. 2001. Dinosaurian growth patterns and rapid avian growth rates. Nature 412:429–433.

Filla J, Redman PD. 1994. *Apatosaurus yahnahpin*: Preliminary description of a new species of diplodocid sauropod from the Late Jurassic Morrison Formation of southern Wyoming, the first sauropod dinosaur found with a complete set of "belly ribs" Fieldguide fourty-fourth Annual Field Conference Wyoming Geological Association. p 159–178.

Foster JR. 2005. New juvenile sauropod material from Western Colorado, and the record of juvenile sauropods from the Upper Jurassic Morrison Formation. In: Tidwell V, Carpenter K, editors. Thunder-lizards. The sauropodomorph dinosaurs. Bloomington and Indianapolis: Indiana University Press. p 141–153.

Geist NR, Jones TD. 1996. Juvenile skeletal structure and the reproductive habits of dinosaurs. Science 272:712–714.

Gillette DD. 1991. *Seismosaurus halli*, gen. et sp. nov., a new sauropod dinosaur from the Morrison Formation (Upper Jurassic/Lower Cretaceous) of New Mexico, USA. J Vert Paleontol 11:417–433.

Gilmore CW. 1925. A nearly complete articulated skeleton of *Camarasaurus*, a saurischian dinosaur from the Dinosaur National Monument. Memoirs Carnegie Mus 10:347–384.

Gilmore CW. 1936. Osteology of *Apatosaurus* with special reference to specimens in the Carnegie Museum. Memoirs Carnegie Mus 11:175–300.

Hanna RR. 2002. Multiple injury and infection in a sub-adult theropod dinosaur *Allosaurus fragilis* with comparisons to allosaur pathology in the Cleveland-Lloyd Quarry collection. J Vert Paleontol 22:76–90.

Harris JD. 2006a. Cranial osteology of *Suuwassea emilieae* (Sauropoda: Diplodocoidea: Flagellicaudata) from the Upper Jurassic Morrison Formation of Montana, USA. J Vert Paleontol 26:88–102.

Harris JD. 2006b. The axial skeleton of the dinosaur *Suuwassea emilieae* (Sauropoda: Flagellicaudata) from the Upper Jurassic Morrison Formation of Montana, USA. Palaeontology 49:1091–1121.

Harris JD, Dodson P. 2004. A new diplodocoid sauropod dinosaur from the Upper Jurassic Morrison Formation of Montana, USA. Acta Palaeontologica Polonica 49:197–210.

Hasiotis S, Fiorillo AR, Hanna RR. 1999. Preliminary report on borings in Jurassic dinosaur bones: Evidence for invertebrate-vertebrate interactions. Utah Geol Surv Misc Publ 99-1:193–200.

Hatcher JB. 1901. *Diplodocus* (Marsh): Its osteolology, taxonomy, and probable habits, with a restoration of the skeleton. Memoirs Carnegie Mus 1:347–355.

Hatcher JB. 1903. Osteology of *Haplocanthosaurus*, with description of new species and remarks on probable habits of the Sauropoda, and the age and origin of the *Atlantosaurus* beds. Memoirs Carnegie Mus 2:1–72.

Hogg DA. 1984. The development of pneumatization in the postcranial skeleton of the domestic fowl. J Anat 139:105–113.

Holland WJ. 1906. The osteology of *Diplodocus* Marsh. Memoirs Carnegie Mus 2:225–278.

Holtz TRJ, Chapman RE, Lamanna MC. 2004. Mesozoic biogeography of dinosauria. In: Weishampel DB, Dodson P, Osmolska H, editors. The dinosauria. Berkeley: University of California Press. p 627–642.

Horner JR, Currie PJ. 1994. Embryonic and neonatal morphology and ontogeny of a new species of *Hypacrosaurus* (Ornithischia, Lambeosauridae) from Montana and Alberta. In: Carpenter K, Hirsch KF, Horner JR, editors. Dinosaur eggs and babies. Cambridge: Cambridge University Press. p 312–336.

Horner JR, de Ricqlès AJ, Padian K. 1999. Variation in dinosaur skeletochronology indicators: Implications for age assessment and physiology. Paleobiology 25:295–304.

Horner JR, de Ricqlès AJ, Padian K. 2000. Long bone histology of the hadrosaurid dinosaur *Maiasaura peeblesorum*: Growth dynamics and physiology based on an ontogenetic series of skeletal elements. J Vert Paleontol 20:115–129.

Ikejiri T. 2003. Sequence of closure of neurocentral sutures in *Camarasaurus* (Sauropoda) and implications for phylogeny in Reptilia. J Vert Paleontol 23:65A.

Ikejiri T. 2004a. Anatomy of *Camarasaurus lentus* (Dinosauria: Sauropoda) from the Morrison Formation (Late Jurassic), Thermopolis, central Wyoming, with determination and interpretation of ontogenetic, sexual dimorphic, and individual variation in the genus, Master thesis, Fort Hays State University.

Ikejiri T. 2004b. Relative growth and timing of ontogenetic changes in *Camarasaurus* (Dinosauria Sauropoda). J Vert Paleontol 24:74A.

Ikejiri T. 2005. Distribution and biochronology of *Camarasaurus* (Dinosauria, Sauropoda) from the Jurassic Morrison Formation of the Rocky Mountain Region. New Mexico Geological Society 56th field Conference Guidebook, Geology of the Chama Basin p. 367–379.

Ikejiri T, Schwarz D, Breithaupt BH. 2005a. A nearly complete skeleton of a baby sauropod from the Lower Morrison Formation of the Howe Stephens Quarry, Wyoming: "little steps" into diplodocid ontogeny and taxonomy. J Vert Paleontol 25:73A.

Ikejiri T, Tidwell V, Trexller DL. 2005b. New adult specimens of *Camarasaurus lentus* highlight ontogenetic variation within the species. In: Tidwell V, Carpenter K, editors. Thunder-lizards. The sauropodomorph dinosaurs. Bloomington: Indiana University Press. p 154–179.

Janensch W. 1950. Die Wirbelsäule von *Brachiosaurus brancai*. Palaeontographica (Suppl. 7):27–92.

Jensen JA. 1985. Three new sauropod dinosaurs from the Upper Jurassic of Colorado. Great Basin Nat 45:697–709.

Jensen JA. 1987. New brachiosaur material from the Late Jurassic of Utah and Colorado. Great Basin Nat 47:710–720.

Laws RR, Hasiotis S, Fiorillo AR, Chure DJ, Breithaupt BH, Horner JR. 1996. The demise of a Jurassic Morrison dinosaur after death—Three cheers for the dermistid beetle. Geol Soc Am Abs Progr 28:A-299.

Lehman TM, Coulson AB. 2002. A juvenile specimen of the sauropod dinosaur *Alamosaurus sanjuanensis* from the Upper Cretaceous of Big Bend National Park. Texas. J Paleontol 76:156–172.

Lovelace D, Hartman S, Wahl W. 2005. Revised osteology of *Supersaurus vivianae*. J Vert Paleontol 25:84A–85A.

Lull RS. 1919. The sauropod dinosaur *Barosaurus* Marsh. Mem Conn Acad Arts Sci 6:1–42.

Marsh OC. 1896. The dinosaurs of North America U.S. Geological Survey, Sixteenth Annual Report, p 133–415

Marsh OC. 1898. On the families of sauropodous dinosaurs. Am J Sci 6(4):487–488.

Martin V. 1994. Baby sauropods from the Sao Khua-formation (Lower Cretaceous) in northeastern Thailand. Gaia 10:147–153.

Martin V, Buffetaut E, Suteethorn V. 1994. A new genus of sauropod dinosaur from the Sao Khua formation (Late Jurassic Early Cretacous) of northeastern Thailand. Comptes Rendus l'Acad Sci Paris (II) 319:1085–1092.

McIntosh JS. 1981. Annotated catalogue of the dinosaurs (Reptilia: Archosauria) in the collections of the Carnegie museum of natural history. Bull Carnegie Mus Nat Hist 18:1–67.

McIntosh JS. 1990a. Sauropoda. In: Weishampel DB, Dodson P, Osmolska H, editors. The dinosauria. Berkeley: University of California Press. p 345–401.

McIntosh JS. 1990b. Species determination in sauropod dinosaurs with tentative suggestions for their classification. In: Carpenter K, Currie PD, editors. Dinosaur systematics. Approach and perspective. New York: Cambridge University Press. p 53–96.

McIntosh JS. 2005. The Genus *Barosaurus* Marsh (Sauropoda, Diplodocidae). In: Tidwell V, Carpenter K, editors. Thunder-lizards. The Sauropodomorph Dinosaurs. Bloomington and Indianapolis: Indiana University Press. p 38–77.

McIntosh JS, Miller WE, Stadtman KL, Gillette DD. 1996. The osteology of *Camarasaurus lewisi* (Jensen, 1988). Brigham Young University Geology Studies 41:73–115.

Michelis I. 2002. Vergleichende Taphonomie des Howe Quarry (Morrison-formation, oberer Jura), Ph.D thesis, Rheinische Friedrich-Wilhelms Universität.

Mohabey DM. 1987. Juvenile sauropod dinosaurs from Upper Cretaceous Lamenta Formation of Panchmahals District, Gujarat, India. J Geol Soc India 30:210–216.

Müller B. 1908. The air sacs of the pigeon. Smithson Misc Coll 50:365–414.

O'Connor MP. 2003. Pulmonary pneumaticity in extant birds and extinct archosaurs, PhD thesis, Stony Brook University (US).

O'Connor MP. 2006. Postcranial pneumaticity: An evaluation of soft-tissue influences on the postcranial skeleton and the reconstruction of pulmonary anatomy in archosaurs. J Morphol 267:1199–1226.

O'Connor MP, Claessens LPAM. 2005. Basic avian pulmonary design and flow-through ventilation in non-avian theropod dinosaurs. Nature 436:253–256.

Osborn HF. 1899. A skeleton of *Diplodocus*. Memoirs Am Mus Nat Hist 1:191–214.

Ostrom JH, McIntosh JS. 1966. Marsh's dinosaurs. New Haven: Yale University Press.

Padian K, de Ricqlès AJ, Horner JR. 2001. Dinosaurian growth rates and bird origins. Nature 412:405–408.

Padian K, Horner JR, de Ricqlès AJ. 2004. Growth in small dinosaurs and pterosaurs: The evolution of archosaurian growth strategies. J Vert Paleontol 24:555–571.

Perry SF, Reuter C. 1999. Hypothetical lung structure of *Brachiosaurus* (Dinosauria: Sauropoda) based on functional constraints. Mitteilungen aus dem Museum für Naturkunde Berlin, Geowissenschaftliche Reihe 2:75–79.

Perry SF, Sander PM. 2004. Reconstruction of the evolution of the respiratory apparatus in tetrapods. Resp Physiol Neurobiol 144:125–139.

Peterson OA, Gilmore CW. 1902. *Elosaurus parvus*, a new genus and species of Sauropoda. Annals Carnegie Mus 1:490–499.

Rauhut OWM, Remes K, Fechner R, Cladera G, Puerta P. 2005. Discovery of a short-necked sauropod dinosaur from the Late Jurassic period of Patagonia. Nature 435:670–672.

Riggs ES. 1903. *Brachiosaurus altithorax*, the largest known dinosaur. Am J Sci 4:299–306.

Russell DA. 1989. An odyssey in time: The dinosaurs of North America. Toronto: University of Toronto Press.

Salgado L. 1999. The macroevolution of the Diplodocimorpha (Dinosauria; Sauropoda): A developmental model. Ameghiniana 36:203–216.

Sander PM. 1999. Life history of Tendaguru sauropods as inferred from long bone histology. Mitteilungen aus dem Museum für Naturkunde Berlin, Geowissenschaftliche Reihe 2:103–112.

Sander PM. 2000. Longbone histology of the Tendaguru sauropods: Implications for growth and biology. Paleobiology 26:466–488.

Sander PM, Tückmantel C. 2003. Bone lamina thickness, bone apposition rates, and age estimates in sauropod humeri and femora. Paläontol Z 77:161–172.

Schwarz D, Frey E, Meyer CA. 2004. The inflated sauropod—distribution and development of pneumatic structures in the cervical vertebrae of *Diplodocus* (Sauropodomorpha) 2nd EAVP meeting, Abstracts, p 29.

Sereno PC, Beck AL, Dutheil B, Larsson HCE, Lyon GH, Moussa B, Sadleir RW, Sidoe CA, Varriccio DJ, Wilson B, Wilson JA. 1999. Cretaceous sauropods from the Sahara and the uneven rate of skeletal evolution among dinosaurs. Science 286:1342–1347.

Swierc JE, Johnson GD. 1996. A local chronostratigraphy for the Morrison Formation, northeastern Bighorn Basin, Wyoming. In: Bowen CE, Kirkwood SC, Miller TS, editors. Resources of the Bighorn Basin: Forty-seventh annual field conference guidebook. Casper. p 315–327.

Tidwell V, Wilhite RD. 2005. Ontogenetic variation and isometric growth in the forelimb of the early cretaceous sauropod *Venenosaurus*. In: Tidwell V, Carpenter K, editors. Thunder-lizards. The sauropodomorph dinosaurs. Bloomington: Indiana University Press. p 187–196.

Turner CE, Peterson F. 1999. Biostratigraphy of dinosaurs in the Upper Jurassic Morrison Formation of the Western Interior, USA. Utah Geological Survey Miscellaneous Publication 99-1:77–114.

Upchurch P. 1998. The phylogenetic relationships of sauropod dinosaurs. Zoo J Linn Soc Lond 124:43–103.

Upchurch P, Barrett PM, Dodson P. 2004a. Sauropoda. In: Weishampel DB, Dodson P, Osmolska H, editors. The dinosauria. Berkeley: University of California Press. p 259–322.

Upchurch P, Tomida Y, Barrett PM. 2004b. A new specimen of *Apatosaurus ajax* (Sauropoda: Diplodocidae) from the Morrison Formation (Upper Jurassic) of Wyoming, USA. Natl Sci Mus Monogr 26:1–107.

Wedel MJ. 2003a. The evolution of vertebral pneumaticity in sauropod dinosaurs. J Vert Paleontol 23:344–357.

Wedel MJ. 2003b. Vertebral pneumaticity, air sacs, and the physiology of sauropod dinosaurs. Paleobiology 29:243–255.

Wedel MJ, Cifelli RI, Sanders RK. 2000a. Osteology, paleobiology, and relationships of the sauropod dinosaur *Sauroposeidon*. Acta Palaeontol Pol 45:343–388.

Wedel MJ, Cifelli RI, Sanders RK. 2000b. *Sauroposeidon proteles*, a new sauropod from the Early Cretaceous of Oklahoma. J Vert Paleontol 20:109–114.

Wedel MJ, Sanders RK. 2002. Osteological correlates of cervical musculature in Aves and Sauropoda (Dinosauria: Saurischia), with comments on the cervical ribs of *Apatosaurus*. PaleoBios 22:1–6.

Weishampel DB, Barrett PM, Coria RA, Le Loeuff J, Ying X, Xijin Z, Sahni A, Gomani EMP, Noto CR. 2004. Dinosaur distribution. In: Weishampel DB, Dodson P, Osmolska H, editors. The dinosauria. Berkeley: University of California Press. p 517–613.

Wilhite RD. 1999. Ontogenetic variation in the appendicular skeleton of the genus *Camarasaurus* Master Thesis, Brigham Young University.

Wilhite RD. 2005. Variation in the appendicular skeleton of North American sauropod dinosaurs: Taxonomic implications. In: Tidwell V, Carpenter K, editors. Thunder-lizards. The sauropodomorph dinosaurs. Bloomington: Indiana University Press. p 268–301.

Wilhite RD, Curtice BD. 1998. Ontogenetic variation in sauropod dinosaurs. J Vert Paleontol 18:86A.

Wilson JA. 1999. A nomenclature for vertebral laminae in sauropods and other saurischian dinosaurs. J Vert Paleontol 19:639–653.

Wilson JA. 2002. Sauropod dinosaur phylogeny: Critique and cladistic analysis. Zoo J Linn Soc 136:217–276.

Wilson JA, Sereno PS. 1998. Early evolution and higher-level phylogeny of sauropod dinosaurs. J Vert Paleontol Mem 5 18:1–68.

Witmer LM. 1997. The evolution of the antorbital cavity in archosaurs: A study in soft-tissue reconstruction in the fossil record with analysis of the function of pneumaticity. J Vert Paleontol Mem 3 17:1–73.

Yates AM, Vasconcelos CC. 2005. Furcula-like clavicles in the prosauropod dinosaur *Massospondylus*. J Vert Paleontol 25:466–468.

Zhang Y, Yang D, Peng G. 1984. New materials of *Shunosaurus* from the Middle Jurassic Dashanpu, Zigong, Sichuan. J Chengdu College Geol (Suppl. 2):1–12.